Extending the Capabilities of Time-Delayed Haptic Teleoperation Systems

Daniel W. Budolak

Thesis submitted to the Faculty of the
Virginia Polytechnic Institute and State University
in partial fulfillment of the requirements for the degree of

Master of Science
in
Mechanical Engineering

Alexander Leonessa, Chair
Alfred L. Wicks
Kaveh Akbari Hamed

February 20, 2020
Blacksburg, Virginia

Keywords: Robotics, teleoperation, time-delay, semi-autonomous control, series elastic actuation (SEA), adaptive parameter estimation

Extending the Capabilities of Time-Delayed Haptic Teleoperation Systems

Daniel W. Budolak

(ABSTRACT)

This thesis focuses on making improvements to time-delayed teleoperation systems, with both direct and semi-autonomous haptic control, by addressing the challenges associated with force-position (F-P) predictive architectures. As the time delay from the communication channel increases, system stability and performance degrade. Previously, solutions focused on communication channel stability and environment force estimation methods that primarily rely on linearization of the Hunt-Crossley (HC) contact model. These result in a loss of transparency in the system and limiting use cases from linearization assumptions. Moreover, semi-autonomous solutions aimed at decreasing user effort and automating subtasks, such as obstacle avoidance and user guidance, require training or singularly focus on joint space tasks. This work addresses the shortcomings of the aforementioned methods by refocusing on system components to achieve more favorable dynamics during environment contact with the use of a series elastic actuator (SEA), investigating alternative HC parameter estimation techniques, and synthesizing an assistive semi-autonomous control framework that predicts user intention recognition and automates gross motion tasks. Experimental results with a remote SEA demonstrate improved performance with stiff environments in delays of up to two seconds round trip time. The coupling of the force and position through the actuator along with simultaneous sensing capabilities also show robustness for contact with soft environments. Further improvements with soft environment contact are achieved through HC parameter estimation, with smooth parameter update switching using a Sigmoid function. A novel application of Chebyshev polynomial approximation for adaptive parameter estimation of the HC model was also proposed. This approach provides control via backstepping with adaptive parameter estimation using Lyapunov methods. Additionally, this method reduces excitation requirements by using nonlinear swapping and the data accumulation concept to guarantee parameter convergence. A simulated teleoperation system demonstrates the effectiveness of this approach and initial results from experiment show promise for this approach in practice. Finally, a user study involving a pick and place task produced favorable results for the proposed semi-autonomous framework which significantly reduced task completion times.

Extending the Capabilities of Time-Delayed Haptic Teleoperation Systems

Daniel W. Budolak

(GENERAL AUDIENCE ABSTRACT)

Teleoperated systems are powerful solutions for remotely executing tasks in situations where autonomous solutions are not robust enough and/or user knowledge is desired for a task. However, teleoperation performance and stability is degraded by delays in the communication channel. A common way to deal with time delay is to use a predictive controller on the local side to cancel out the delay by knowing the remote side dynamics. Previous approaches have focused on stabilizing the communication channel or the use of estimators and observers to better capture the remote side dynamics. The drawback of these approaches is that they achieve stability at the expense of system transparency, leading to divergence in the force and position matching between the master and remote side. Many of the methods for environment force estimation involves linearizing contact models, creating limitations in their application. Moreover, semi-autonomous solutions aimed at decreasing user effort and automating subtasks such as obstacle avoidance and user guidance require training data sets for the algorithm or only focus individually on joint space tasks. This thesis addresses the shortcomings of the aforementioned methods by refocusing on system components to achieve more favorable dynamics using a series elastic actuator (SEA) while interacting with the environment, investigating nonlinear and linear contact model estimation methods for identifying parameters of the Hunt-Crossley (HC) model, and synthesising an assistive semi-autonomous control framework that predicts user intention for task execution. Experimental results for the use of an SEA demonstrate improved performance with stiff environments in delays of up to two seconds round trip time (RTT). The coupling of the force and position through the actuator along with simultaneous sensing capabilities also showed robustness for contact with soft environments. Various estimation methods for HC parameter identification was investigated to improve the local side model. A novel application of Chebyshev polynomial approximation of the HC model with adaptive parameter estimation was also proposed to provide control along with decreasing the excitation requirements by using backsteping control with nonlinear swapping and the data accumulation concept. A simulated teleoperation system demonstrated the effectiveness of this approach with a smooth paramater update transition. Initial results from experiment also show promise for this approach in practice. Finally, a user study involving a pick and place task produced favorable results for the proposed semi-autonomous framework which significantly reduced task completion times.

Contents

List of Figures

List of Tables

Chapter 1

Introduction

Extending the capabilities of teleoperated systems remains a critical research topic for tasks that need to leverage user knowledge in remote or inaccessible environments. Additionally, current autonomous solutions are not robust enough to handle unstructured or changing environments and tasks. Advancements in this area are beneficial to applications in telesurgery, space operations, subsea, and generally remote tasks when a human operator desired but the environment is not hospitable [1, 2].

Teleoperation systems consist of a device for user input, referred to as the master on the local side, and a remote robot or slave machine. This work will refer to the slave side as "remote" or "follower". Communication between the master and follower side can be wired, but for very remote operation will be based on wireless or internet protocol (IP) communication. In bilateral haptic systems, the follower robot mimics the motion or input of the user and sends back the force that is exerted on it from interaction with an environment. The master device then reflects that force back onto the user. The ultimate goal of many teleoperated systems is telepresence, or providing the user a sense of being in and interacting with the environment. Typically, architectures such as these are referred to as 2 channel force-position (F-P) systems since a position command is sent to the follower and the environment force is reflected back on to the user, as depicted in Fig. 1.1. Many other architectures exist that utilize various control and communication schemes to address the particular application.

The ability to execute tasks with expert knowledge remotely has significant advantages with a multitude of applications as previously mentioned. However, as the physical distance between the master and remote side increases, many challenges surface as a result of the associated communication delay. Namely, decreased stability and performance. Although various solutions have been investigated to mitigate these challenges many limitations persist. The topics herein address these limitations by focusing on minimizing transparency loss, providing better online environmental contact force estimation for predictive control

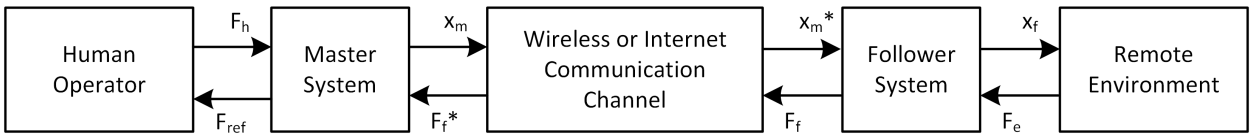

Figure 1.1: Common 2-Channel Force-Position Teleoperation System.

methods, and implementing user intention prediction with semi-autonomous assistance. The following section reviews previous work done to extend teleoperation capabilities, highlighting remaining challenges or limitation, and noting potential solutions this work addresses.

1.1 Literature Review

1.1.1 Effects of Time Delay

The greatest challenge of teleoperated systems is dealing with time delay from the communication channel. The further away the remote side is, the longer it takes for a signal to be sent and received. Thus, when a command is sent to the remote side, by the time the response is sent back to the operator the target has been overshot. This leads to operator induced oscillations that make the system hard to control. Time delay also can lead to instabilities since the delay, e^{-sT} will reduce the phase margin in the control scheme from a classical perspective. This leads to oscillations and eventually instability as the delay increases. These effects of time delay on a system are shown in Fig. 1.2. Time delay can be constant or time varying, as well as asymmetrical, where the forward delay may not be equal to the backward delay. When the communication is over internet, packet losses, bandwidth limitations, and jitter can also affect the time varying dynamics of delay and lead to instabilities. Methods to deal with the nonlinear and time-varying effects of internet communication have been studied in [3, 4, 5]. Notably in [4], time varying delays and IP communication with jitter can be turned into constant delays with the use of buffering and network delay regulation.

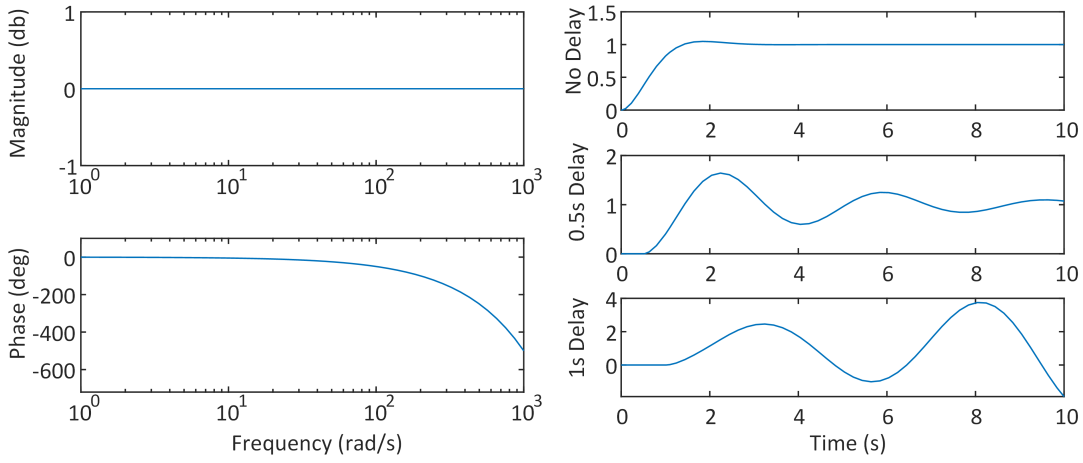

Figure 1.2: Bode plot for time delay: e^{-sT}, T = 0.5 s [left]. Second order system output with proportional control: no delay, 0.5 s delay, and 1 s delay [right].

1.1.2 Transparency & Passivity

To overcome the destabilizing affects of the communication delay, various stability guaranteeing control methods have been investigated. However, the guarantee of stability is achieved at the expense of transparency. Transparency is the performance metric of teleoperated systems and is achieved through position and force matching, such that $x_{\mathrm{h}} = x_{\mathrm{e}}$ and $F_{\mathrm{h}} = F_{\mathrm{e}}$, where the subscripts h and e refer to the human operator and environment.

In early studies, transparency was focused on matching the impedance transmitted to the operator (Z_{h}) to the environment impedance (Z_{e}) such that $Z_{\mathrm{h}} = Z_{\mathrm{e}}$. A 4-Channel (4C) approach was proposed where both force and velocity signals are transmitted [6]. In this manner, the impedance of the master and remote system can be matched as knowledge of the force and velocity is transmitted. However, the transparency is achieved at the expense of passivity, that is, stability through energy bounding of signals. To guarantee passivity, the common two channel method was developed, but with a loss of transparency [7]. This asserts that transparency and passivity are opposing goals that researchers continue to combat. The two channel architecture is depicted in Fig.1.1 where F and x denote the force and position signals, and subscripts h, m, f, and ref refer to the human, master, follower, and reflected signal.

Passivity was first presented for teleoperation systems with scattering variables by [8]. The concept of passivity can be simply demonstrated by examining a two port network where the energy entering the system must be greater than or equal to the energy leaving the system for all time,

$$\int_0^\infty F^{\mathrm{T}}(t)v(t)\mathrm{d}t \geq 0.$$

Passivity provides a convenient and conservative assurance of stability, and thus has been widely implemented through transformation variables applied to signals sent through the communication channel. The use of wave variables (WV) in particular has become very popular since it guarantees stability regardless of the time delay and follower side dynamics. However, because no position information is explicitly available, position drift is a common consequence. A detailed discussion on the benefits and limitations of WV is presented in [9]. Enforcing passivity can also be extended to other parts of the system. This was notably done in [10], using a proportional-derivative (PD) control over the delayed communication channel and passifying the communication and control blocks together. This framework showed promise particularly in being able to handle different time delays in the forward and backward delays, as long as the round trip was constant and upper bounded. However, in larger time delays significant error in position and force reflection was reported.

WV have also been notably used to stabilize the H_∞ controller in [11]. This study performed a pick and place telemanipulation task between the USA and Japan in an RTT of 0.48s, with the help of voice queues from the follower side. The teleoperation system consisted

of a haptic exoskeleton glove and manipulator. Although this work successfully presented a practical demonstration of haptic teleoperation system, it was constrained to a small delay. Additionally, the system features the common performance and stability trade-off for passivity approaches.

Other methods to improve transparency have also been investigated. One such method involves predicting the user input by examining the operator and haptic interface dynamics such as in [12]. In this work, the human input is predicted with minimum jerk motion models. Similarly, [13] used impedance based force control on the master to compensate for the dynamics of the haptic device.

1.1.3 Predictive Control Methods

One very successful way of dealing with time delay is through the use of predictive control methods. For instance, with the use a model predictive controller (MPC), if the remote side dynamics are known, then a control signal can be constructed through optimization that produces the desired output despite a time delay. Similarly, a variation of this known as a Smith Predictor (SP) [14] can be used to cancel out the time delay in the system from knowledge of the remote side dynamics. Using these methods, the user on the master side perceives no delay due to the control strategy generating a predicted remote side force. The greatest challenge in predictive control approaches is obtaining an accurate model or estimation of the follower and environment, particularly when the follower and environment dynamics are nonlinear or time varying. The consequences for model based methods are that any modeling errors or unaccounted disturbances and nonlinearities can degrade performance and destabilize the system. This comes as a result of time delayed signals not being accuratly canceled out. To address this [15, 16] use online neural networks (NN) to estimate follower side dynamics. As an online method, the NN can respond to small changes in the follower and environment dynamics, however, it requires training and the weights require sufficient time to converge.

Others have addressed the concerns with predictive methods by using adaptive model based approaches and observers, such as in [17, 18, 19]. From the most recent example, the improved extended active observer in [19] relies on accurate rigid body models and observers to estimate the external and friction torques of the system. This approach, like most adaptive methods, can handle variations in the communication delay but is limited to small delay times and its ability to adapt to varying environment dynamics has not been investigated.

One of the great benefit of predictive control methods is that they are modular; passivity, stability controllers, and error bounding methods can be combined and applied on top of the control architecture. Additionally, as shown in some of the works mentioned above, the remote model can be replaced with estimators. In this manner, the energy bounding approach (EBA) can be used to achieve passivity without scattering or WV [20]. Here the concept of passivity is applied as a controller to bound energy output on both the master

and follower. This method was expanded in [21] where the bilateral EBA was combined with an Smith predictor F-P architecture. Similar to [10], this method guaranties stability but has the common stability-performance trade-off since the EBA bounds the force magnitude on the master side. Like many approaches, the predictive EBA also needs to know the environment dynamics to have good transparency. Alternatively, [22] used a sliding mode based finite time controller with a barrier Lyapunov function to address performance and stability, with a NN for uncertainties. This has promising results with its ability to constrain the position error, but has not been applied to environment interaction, and no results have been provided for force matching.

1.1.4 Environmental Contact Force Modeling

Oftentimes in real world applications the environment impedance does not stay constant, can have time varying dynamics, or is unknown. Thus, static a priori models are often insufficient for obtaining the desired level of transparency. To address this shortcoming, estimation methods can be used to obtain and update the environment model or parameters in real time. Many have implemented observers in the control scheme to accomplish this such as in [23]. These and similar observer methods estimate external forces and torques acting on the system from knowledge of the system models, often reducing the need for force or velocity sensors. However, they are sensitive to unmodeled dynamics, inertia, and friction. These shortcomings were addressed in [19] by including external force estimation and disturbance suppression. Although this showed improvements, as previously mentioned, this requires accurate knowledge of the rigid body dynamics. Moreover, although there is adequate force tracking performance in delays up to 0.2s, position tracking cannot be achieved when there is torque input to the haptic device. A different approach to observer implementation is used in [24] where a modified Kalman filter is used with stochastic methods for disturbance estimation. This method achieves good performance in experiments, however, it uses a postion-position architecture that relies on coupling through a virtual gain and scaling for the position and virtual force. The limitation of this method lies in the need to use adaptive methods to find the gain so that the haptic feel quality of stiff objects does not degrade. Other methods focus on estimating the stiffness of the environment model to get impedance matching such as in [25]. Like many other prediction based methods, the model of the environment on the master side is updated from the remote side. In this control scheme, a gradual update for stiffness parameters was also incorporated when switching between objects of different impedance to avoid spikes in the reflective force. However, this method used a linear environment model limiting its practical application.

Similar to estimating stiffness for impedance matching, it may be more useful to to estimate the environment contact force based on the material properties of an object. The most common and effective way of achieving this is through the use of a contact model. Typically, a continuous contact model is implemented, such as the Hunt-Crossley (HC) [26] contact model, or other application specific ones (e.g. soft tissue models for telesurgery). For contact

models to be effective, the parameters of the material needs to be known a priori. However, if the material is unknown or the task changes, these parameters need to be determined online such that the model adapts to the material without prior knowledge. The aforementioned NN estimation approaches [15, 16] attempted to do just that. Alternatively in [27], a self-perturbing recursive least squares estimation was use to identify the parameters of the HC as well as the linear Kelvin-Voigt model. This work obtained good force estimation with a control scheme that switches between the two models given the contact velocity to not violate the convenient linearization of the HC method provided by [28]. However, this work did not incorporate any time delay in the experiment. In [29], the previous work in [28] is extended to practical contact experiments with the use of an exponentially weighted recursive least squares estimator (EWRLS). However, to satisfy the linearization assumptions and provide good accuracy, the velocity of the contact is limited to a threshold value. Similar work was done in [30] where EWRLS was used with a modified Hiddadi linearization using Taylor series expansion. In this approach, the Lankarani and Nikravesh contact model is used instead of the HC. This showed improved robustness to error but had long convergence times with soft materials. Another method [31], proposed approximating the nonlinear exponential term in the HC model with a quadratic polynomial. This provided a convenient method for approximating the model without the drawbacks of the Haddadi method that still allowed the use of least squares estimation. However, the performance is limited to the the number of polynomial terms used for estimation, which in turn has a greater requirement of excitation for convergence.

Using recursive least squares (RLS) is very popular for estimation problems due to its simplicity. The main drawback is that it requires a linear parametric model. This is why Haddadi's linearization method has become so prevalent in estimating the HC model. To avoid limitations of linear approximation, others have pursued Kalman filtering approaches for parameter and state estimation. The benefit of using an extended Kalman filter (EKF) is that it is formulated specifically to handle small nonentities and is often used for parameter estimation. The work in [32] showed promising results using an EKF for a nonlinear tissue dynamics model. More recent work in [33] used a variation of the EKF termed the uncented Kalman filter (UKF) for estimating the contact force of the HC model. Their work compared using a UKF with their proposed random waiting and strong tracking UKF, that also showed improved performance, with slightly larger convergence times than in [32]. Many of these methods show promise in practical online environmental force estimation. However, the greatest limitation in all of these studies is that they have not been implemented to estimate the parameters of the HC model, only the force is estimated without parameter convergence. This limits its use for predictive based controllers. Thus, there still remains work to establish the most efficient way to estimate the environment interaction force in real time for time delayed systems.

Alternatively to the examined estimation methods, adaptive methods can also be employed to derive update laws for parameter estimation as well as provide control laws for stabilizing the remote system. The groundwork for this is laid out and discussed at length in the

approach provided by [34]. The use of backstepping provides input to state stability, while implementation of nonlinear swapping provides a convenient formulation for parameter estimation with common gradient or least square update laws. As discussed previously, a more robust parameter identification method is desired. A promising solution is provided in the work by [35] that uses nonlinear swapping with Lyapunov based methods to guarantee parameter convergence. Morover, this approach relaxes the persistent excitation requirement by modifying the update law to make the Lyapunov derivative negative definite with respect to the parameter estimation error. However, this work was only examine for an inverted pendulum in simulation, and has yet to be applied to environment parameter identification or a teleoperated system.

1.1.5 Compliance in the Teleoperation System and SEAs

Earlier work in teleoperation has also investigated shared compliance control (SCC) [6]. It was recognized that compliance on the follower side is beneficial for safely controlling the remote robot. However, at the time, manipulator stiffness was preferred for positional accuracy. Thus, compliance was actively achieved through impedance control despite certain advantages of passive compliance. One such known advantage is the use of remote compliant center (RCC) wrists in manipulators [36]. Because of this, passive compliance remains mainly unexplored in teleoperation, despite many potential benefits that can be applied in the form of a series elastic actuator (SEA).

SEA's have many advantages over direct drive actuators including accurate force control, and reduced force errors from friction and torque ripples that can cause position drift [37]. Moreover, the unified force through position control of SEA's lends itself very well to the F-P architecture in teleoperation. Compliant robots are also becoming increasingly more popular in both research and industry as safe human interaction is becoming a critical concern. The main method of ensuring safe operation is minimizing inertial forces and enforcing compliance by passive means with SEA's instead of active control. The reason being compliance in the actuator reduces the reflected inertia [37, 38]. A new robot design in [39] showcases the importance and the benefits of passive joint compliance through SEA's in contact detection as well as unified force motion control.

Since an SEA functions as a force/torque sensor as well as an actuator, contact can be determined by measuring the joint torques while interacting with an unknown environment. This is beneficial for teleoperation as it provides a method to accommodate varying environments. A study by [40] also suggests that the use of SEA's on the follower side may be beneficial in future teleoperation systems. Another study [41] makes note that the effects of compliance in haptic feedback has not been examined thoroughly.

1.1.6 Semi-Autonomous Control & User Intention Prediction

One of the great benefits of teleoperation stems from its ability to leverage operator knowledge to handle unstructured or complex remote tasks that fully autonomous systems are unable to handle. However, as the time delay increases, predictive control methods alone can not fully account for changes or unknowns in the remote environment. For this reason, some autonomy on the remote side is necessary to ensure safe interaction with the environment, such as accounting for drop offs or changes in terrain for mobile applications, or obstacle avoidance.

To increase productivity and reduce user fatigue, some autonomous methods have been applied to augment teleoperation in shared or semi-autonomous control. With these methods the user and robot share or split control over the system states, where the level of control is often handled with confidence weighting. Recent work [42, 43] demonstrates that shared control improves task completion time and is intuitive for users. However, these studies were conducted without time delay.

Current research focuses on how best to incorporate autonomy and identify user input by examining different frameworks and levels of assistance. An important aspect of this is how to identify user intention. Typically, the frameworks are implemented in a supervisory manor where the user defines tasks and targets ahead of operation [44, 45] or hierarchical task control as presented in [46], where the shared control executes sub-tasks autonomously and may or may not assist the main task. Sub task control for redundant manipulators has already been well studied [43, 47, 48, 49]. Typical tasks include monitoring and preventing joint limits, configuration singularities, guiding end-effector orientation, and obstacle avoidance. These are natural candidates for automation to reduce user effort allowing more focus on the higher level objective. Other task assistive methods have been implemented in the form of haptic force reflection for guidance [50, 51]. This is accomplished through impedance based guidance and collision avoidance by use of virtual force fields or a virtual spring and damper connecting the task and end-effector. Impedance based guidance has also been widely used in obstacle avoidance for mobile robots controlled via teleoperation [52, 53, 54]. Many shared control approaches have been adapted from the field of mobile robotics for guidance and collision avoidance in the form of potential fields [55], some with enhanced capabilities of online vision based fixture generation as in [56]. Unfortunately, both impedance and potential fields approaches have drawbacks, as the impedance force can confine the pose by pulling to a task while being repelled by an obstacle, similar to how a potential field may cause the robot to be locked into a local minimum. Other methods have focused on assistance recognition for predicting user motion to move to a target or execute a task. Most often, this is accomplished with a hidden Markov model (HMM) [57, 58]. Some have also used Gaussian processes for implementing shared control from tasks learned by demonstration [59]. The major drawback of such approaches is that they require training, which can be a very time consuming.

Different approaches, like those in [60, 61], identify user intention from their trajectory using

regression to form a line for the expected path and accumulating the distances to targets from the path up to a threshold to determine intention. However, this requires the user to travel along the path for a sufficient amount of time until a target is identified. This will slow down operation, particularly in the presence of obstacles where the path may need to change to avoid collisions. A simplified method is to project the current direction on to the vector from the current end-effector pose to a target. This was done in [62] with a set of heuristics to identify user intent for autonomous execution of grasp primitives. However, in their method, the robot pose had to be sufficiently close to the grasping target, making it's use case more suited for action recognition than target identification. Although autonomous execution of fine movements is beneficial in some applications, it removes some of the user knowledge that can be leveraged in teleoperation. Thus, shared control and autonomous assistance for gross motion can be of greater benefit for reducing user effort and task completion time, particularly where user skill can be used for direct teleoperation. With this control structure, path planning can be leveraged to execute the aforementioned gross motion while avoiding collisions, such as in [63].

Some of the aforementioned methods demonstrate great potential as options for decreasing user effort, but to the knowledge of the authors, they have not been synthesized for a holistic shared control or semi-autonomous framework.

1.2 Research Contribution

Based on an extensive literature review, the current practical limits for bilateral haptic teleoperation is an RTT of approximately 500 ms for precise or dexterous tasks. Performance of teleoperation systems degrades as the delay time increases, particularly for systems that enforce passivity. Solutions such as WV and estimation methods for the transmission delay has made a significant portion of the recent work in this field focus on the communication channel over other parts of the teleoperation system that can be further developed to increase performance. Moreover, few studies have investigated robust solutions to varying environment dynamics. Much work remains for increasing haptic teleoperation performance in large time delays by further examining unexplored components of the system such as environment contact on the follower side. To address these issues this paper presents the novel use of an SEA as a compliant end effector on the follower side. The coupling of the actuator force and position provides improved transparency in time delays of up to two seconds and adaptability to environment position variation. This approach has been show to be particularly effective when implemented with a predictive model based controller on the master side, and compliments the implementation of a F-P architecture.

To achieve better performance with the proposed SEA system, in particular when interacting with a soft environment, the use of the HC model in the predictive controller is proposed. Incorporating this approach in unstructured environments and providing a way to accommodate changing tasks necessitates a method for the proposed control architecture to update the

remote side environment model. In these cases a priori knowledge becomes insufficient with unmodeled dynamics or may simply be unavailable. To this end, this work investigates the feasibility of various online estimation methods for obtaining the environmental contact force in a time delayed teleoperation system. Multiple estimation schemes including output error minimization with gradient descent and Levenberg-Marquardt, least squares, and Kalman filtering were studied for estimation of the nonlinear HC model and various approximations. To provide good performance in force estimation and parameter convergence, without the limitations of previous linearization methods, a new Chebyshev polynomial approximation of the HC model is proposed. Additionally, for a more robust solution to both control and parameter estimation of the remote side, a backstepping controller with Lyapunov based parameter update laws was examined. This scheme modifies the update laws to guarantee a negative definite Lyapunov derivative, thereby relaxing the persistent excitation requirement. For this reason the proposed approach is more suitable to online implementation than other estimation methods. Furthermore, to facilitate smooth transition in parameter updates, shifting authority through a sigmoid function is implemented when new parameter values are sent. In this manner there are no discontinuous changes in the reflected force due to a model update.

As time delay increases degradation in performance is inevitable, particularly in the presence of disturbances. To enhance the system performance in these situations, the use of user intention recognition for guidance and obstacle avoidance with semi-autonomous teleoperation is proposed. The novelty of this work is twofold. First, a projection based predictor for user intention recognition is implemented for target identification based on user motion. Second, a control architecture for gross motion automation with subtask execution is developed for assistive teleoperation based on an optimal trajectory from an assumed path planner. The target identification runs continuously allowing for target correction, with the user controlling shifting between direct teleoperation or assisted control. By focusing on the gross motion, there is no need to realign pose frames as in situations with auto grasping. Moreover, this takes greater advantage of the teleoperation paradigm by leveraging user knowledge to execute complex tasks in unstructured environments, while reducing the burden on the user with trivial motion execution. Sub tasks of bounding workspace locations and singularity avoidance are applied to the user as haptic feedback. A user study for a pick and place operations is conducted to evaluate the proposed method's performance and user perception.

Chapter 2

Mathematical Preliminaries

2.1 Smith Predictor

Due to its simplicity and proven performance, the Smith predictor is the primary method for dealing with time delay. In the Smith predictor, the desired force feedback F_{p}, can be written as

$$F_{\mathrm{p}} = \hat{G}_{\mathrm{p}}(1 - e^{-s\hat{T}})x_{\mathrm{m}} + F_{\mathrm{f}}, \tag{2.1}$$

where $\hat{G}_{\mathrm{p}}$ is the follower dynamics estimate, $\hat{T}$ is the estimated round trip time delay, x_{m} is the position of the master, and F_{f} is the actual force feedback from the follower side

$$F_{\mathrm{f}} = e^{-sT} G_{\mathrm{p}}\, x_{\mathrm{m}}.$$

Substituting this into (2.1) the equation becomes

$$F_{\mathrm{p}} = \hat{G}_{\mathrm{p}}(1 - e^{-s\hat{T}})\, x_{\mathrm{m}} + e^{-sT} G_{\mathrm{p}}\, x_{\mathrm{m}},$$

where G_{p} is the actual follower dynamics and T is the round trip time delay. If the time delay is known, $\hat{T} = T$, and the follower dynamics are perfectly predicted, $\hat{G}_{\mathrm{p}} = G_{\mathrm{p}}$, then the time delay is canceled out and the reflected force becomes

$$F_{\mathrm{p}} = G_{\mathrm{p}}\, x_{\mathrm{m}}.$$

Because no passivity enforcing control is applied to this architecture, the system is only stable when there is full cancellation of the time delayed dynamics, $G_{\mathrm{p}} = \hat{G}_{\mathrm{p}}$, with proper controller selection on the follower side. Thus, stability for the system is dependent on the accuracy of the follower and environment dynamics modeling. When modeling error is present, stability of the teleoperation system can still be guaranteed for a bounded error using Nyquist criteria [64]. From examination of the representative block diagram of an SP in Fig. 2.1, the closed loop transfer function is

$$\frac{y}{x} = \frac{CGe^{-sT}}{1 + C\hat{G} + C\Delta G e^{-sT}},$$

where ΔG is additive modeling error. Based on the Nyquist theorem the system will be stable if $1 + C(j\omega)G(j\omega) > C\Delta G(j\omega)e^{-j\omega T}$. The additive error can be represented as $G(j\omega)\delta G(j\omega)$,

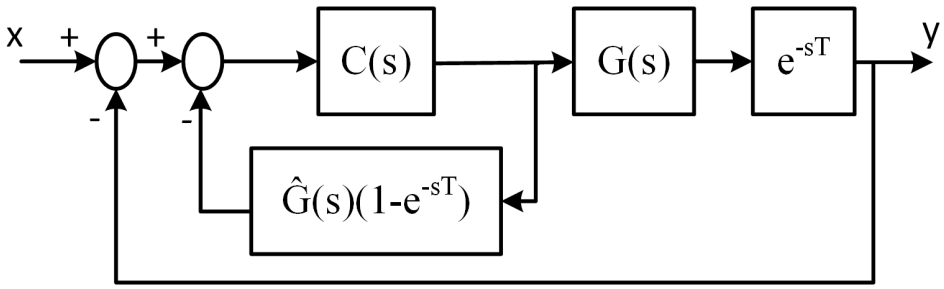

Figure 2.1: A general Smith predictor system with time delay.

where $\delta G(j\omega)$ is the multiplication modeling error. The stability condition now becomes

$$|1 + [C(j\omega)G(j\omega)]^{-1}| > |\delta G(j\omega)e^{-j\omega T}|.$$

Thus, $|\delta G(j\omega)| < W(\omega)$, where $W(\omega)$ is an upper bound function requiring

$$|1 + [C(j\omega)G(j\omega)]^{-1}| > W(w) \quad \forall\, \omega.$$

Therefore, even with modeling error the SP remains stable for the teleoperation system based on the appropriate selection of $C(j\omega)$ for the follower dynamics.

2.2 Unilateral Contact Models

The HC method is well known and widely used to model unilateral contact with various materials. It is particularly good at modeling viscoelastic materials with nonlinear stiffness and damping [29, 65]. The benefit of the HC model is that the normal force F is continuous and takes into account viscous friction forces for elastic conditions based on the contact pseudo penetration δ. Here the force is expressed as

$$F = K_{\mathrm{e}}\delta^n + B_{\mathrm{e}}\delta^n\dot{\delta}, \quad \delta(t) \geq 0. \tag{2.2}$$

K_e is the effective stiffness calculated as

$$K_{\mathrm{e}} = \frac{4\sqrt{R_i}}{3(\sigma_i + \sigma_j)},$$

where $\sigma_* = (1 - v_*^2)/E_*$, for $* = i, j$, where v_* and E_* is the Poisson ratio and Young's modulus respectively, for object i coming into contact with object j. B_{e} is the hysteresis damping factor given by [66] as

$$B_{\mathrm{e}} = \frac{3K_{\mathrm{e}}(1 - c_{\mathrm{r}})}{2\dot{\delta}^{(-)}},$$

where c_r is the coefficient of restitution and $\delta^{(-)}$ is the initial contact velocity. Contact with both a stiff and soft materials can be modeled by changing K_e and c_r, as both are inversely proportional to damping [67].

The HC model is an improvement over the previous standard of the linear Kelvin-Voigt model, $F = k\delta + b\dot{\delta}$ [68], that did not account for the hysteresis in energy dissipation during contact as shown in Fig. 2.2 below.

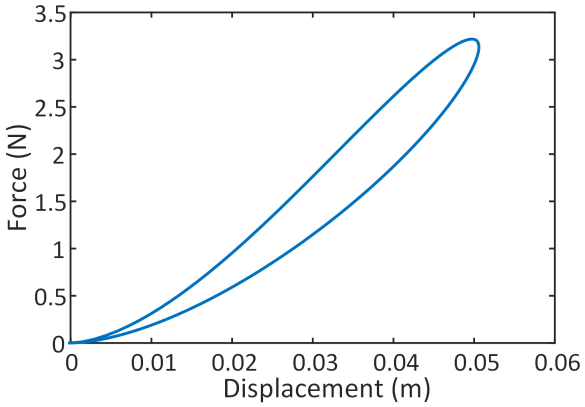

Figure 2.2: Hysteresis curve of HC viscoelastic contact model.

The HC model is also useful because in the degenerate case of no damping it simplifies to the nonlinear elastic Hertz contact model $F = k\delta^n$ [69].

2.3 HC Linearization

This section reviews the method proposed by Haddadi et al in [28] to linearize the HC contact model. The linearization begins by taking the natural logarithm of the HC model after factoring out $K\delta^n$. Because of the logarithm, this method is only valid for $\delta > 0$ which aligns with the HC psudo penetration model.

$$\begin{aligned} \ln[F(t)] &= \ln[K\delta^n(t)(1 + \frac{B\dot{\delta}(t)}{K} + \frac{\epsilon}{K\delta^n(t)})] \\ &= \ln(K) + n\ln[\delta(t)] + \ln[1 + \frac{B\dot{\delta}(t)}{K} + \frac{\epsilon}{K\delta^n(t)}] \end{aligned} \tag{2.3}$$

Taking advantage of $\ln(1+\alpha) \approx \alpha$ for $|\alpha| \ll 1$ and assuming

$$\left|\frac{B\dot{\delta}(t)}{K}+\frac{\epsilon}{K\delta^n(t)}\right| \leq \left|\frac{B\dot{\delta}(t)}{K}\right| + \left|\frac{\epsilon}{K\delta^n(t)}\right| \ll 1,$$

equation (2.3) can be rewritten as

$$\ln[F(t)] \approx \ln(K) + n\ln[\delta(t)] + \frac{B\dot{\delta}(t)}{K} + \frac{\epsilon}{K\delta^n(t)},$$

which is now in a convenient form for least squares estimation

$$y_k = \phi_k^{\mathrm{T}}\theta_k + \bar{\epsilon}_k,$$

where ϕ_k^{T} is the regressor vector and θ_k is the parameter vector being estimated, with $\bar{\epsilon}_k$ representing the modeling error and noise at each iteration. From the Haddadi linearization of the HC model,

$$\phi_k = [1, \dot{\delta}_k, \ln(\delta_k)]^{\mathrm{T}}, \quad \theta_k = [\ln(K), \frac{B}{K}, n]^{\mathrm{T}}, \quad y = \ln(F_k).$$

The original parameters can now be reconstructed as

$$\hat{K} = e^{\theta(1)}, \quad \hat{B} = \hat{K}\theta(2), \quad \hat{n} = \theta(3).$$

However, one major drawback of this method is that it assumes $\frac{B\dot{\delta}(t)}{K} \ll 1$. To ensure this criterion for the linearization the following condition was proposed [29],

$$||\dot{\delta}||_\infty < \frac{0.1K}{B}.$$

This requires that the velocity of the operation be sufficiently small.

2.4 Observability

A system is said to be completely observable if all the states $x(t)$ can be determined in finite time given the outputs $y(t)$. Consider a linear time varying unforced system

$$\begin{aligned} \dot{x}(t) &= A(t)x(t), \quad x(t_0) = x_0, \\ y(t) &= C(t)x(t), \end{aligned}$$

with the unique solution

$$x(t) = \Phi(t, t_0)x_0,$$

where $\Phi(t, t_0)$ is the state transition matrix. This system is uniformly completely observable if its observability Grammian $M(t_0, t_f)$ is uniformly positive definite, i.e.

$$M(t_0, t_f) = \int_{t_0}^{t_f} \Phi^{\mathrm{T}}(t_0, \tau)C^{\mathrm{T}}\Phi(\tau, t_0)d\tau \geq \alpha \mathrm{I} \quad \forall t \geq 0.$$

This means that for the system to be observable, all the columns of $M(t_0, t_f)$ must be linearly independent on $[t_0, t_f]$ [70]. For a linear time invariant (LTI) system where matrices A and C are constant, observability can be seen as the duality of the controllability problem where the $n \times nm$ observability matrix

$$\begin{bmatrix} C^{\mathrm{T}} & A^{\mathrm{T}}C^{\mathrm{T}} & \cdots & (A^{\mathrm{T}})^{n-1}C^{\mathrm{T}} \end{bmatrix},$$

is of rank n.

For nonlinear observability, conditions have mostly been developed for local observability. The most common way of determining nonlinear local observability is by constructing an observabilty matrix by using Lie derivatives of the output [71]. Consider a nonlinear system described by a set of ordinary differential equations

$$\begin{aligned} \dot{x}(t) &= f(x(t)), \quad x(t_0) = x_0, \\ y(t) &= h(x(t)), \end{aligned}$$

where $f : \mathbb{R}^n \to \mathbb{R}^n$ and $h : \mathbb{R}^n \to \mathbb{R}^m$. The observability matrix can be formed by staking Lie derivatives of the output function $h(x)$. A Lie derivatives is defined as

$$L_f^k h(x) = \tfrac{\partial}{\partial x}(L_f^{k-1}h(x))f(x),$$

with $L_f^0 h(x) = h(x)$. Let q be the observability matrix defined as

$$q = \begin{bmatrix} L_f^0 h(x) \\ \vdots \\ L_f^{\kappa-1} h(x) \end{bmatrix},$$

where κ is some minimum number of equations needed to guarantee observability. The system is locally observable if

$$\text{rank } (\frac{\partial q}{\partial x}) = n.$$

All of the observability conditions for states can be extended to parameter identification by treating parameters as states. Or, in the case of simultaneous state and parameter estimation, the parameters θ can be appended to the state vector to form an augmented state and parameter vector $z = [x\ \theta]^{\mathrm{T}}$.

For estimation methods, the observer or filter used must have the estimates converge to the true value. To guarantee parameter convergence, the input(s) to the system must be persistently exciting, to provide sufficient information in all the frequencies of interest. A signal $\nu = [x\ u]^{\mathrm{T}}$ is said to be persistently exciting if there exists an $\alpha > 0$ and $T > 0$ such that for any $t > 0$

$$\int_{t}^{t+T} \nu(\tau)\nu^{\mathrm{T}}(\tau)d\tau > \alpha \mathrm{I}.$$

Persistency of excitation implies that vectors of $\nu(t)$ at different times t are linearly independent.

2.5 Estimation Methods

This section reviews the various estimation methods used for parameter identification. The estimation methods are introduced with the specific algorithm defined.

2.5.1 Output Error Minimization

Gradient Descent

Gradient descent is an adaptive filtering technique that uses a cost function to estimate parameters of a function. The cost function is minimized by searching along the Jacobian, or gradient, of a quadratic cost function towards the minimum. The algorithm is implemented as follows

$$\begin{aligned} r(\theta) &= \frac{1}{2}[z - f(\theta, x)]^2, \\ J_k &= \left.\frac{\partial r}{\partial \theta}\right|_{\theta_k}, \\ \theta_{k+1} &= \theta_k - \alpha J_k, \end{aligned}$$

where $r(\theta)$ is a quadratic cost function consisting of the desired or measured value z_k and the modeled function $f(\theta, x)$, and α is the learning rate.

Levenberg-Marquardt

The Levenberg-Marquardt (LM) method adaptively varies the parameter updates between the gradient descent and Gauss-Newton methods. Using the same quadratic cost function and Jacobian definition as for the Gradient method, the parameter update is given by

$$\begin{aligned} \theta_{k+1} &= \theta_k + h, \\ h &= (J^{\mathrm{T}} J + \lambda I)^{-1} J^{\mathrm{T}} e_k, \end{aligned}$$

where I is the identity matrix, $e_k = z - f(\theta, x)$, and λ is a weighting factor that when large, pushes the update closer to the gradient descent method and towards the Gauss-Newton method when λ is small. After each update, if the iteration improves the approximation $r(\theta + h) < r(\theta)$ λ is decreased, otherwise λ is increased.

Recursive Least Squares

Least squares is an estimation technique that minimizes the squared error of observed date with expected or modeled values. It is commonly used for parameter identification for linearly parameterized model of the form

$$y = \phi^{\mathrm{T}} \theta + \bar{\epsilon},$$

where ϕ^{T} is the regressor vector and θ is the parameter vector being estimated. Minimizing the squared error function

$$J(\theta) = ||y - \phi^{\mathrm{T}} \theta||^2,$$

a unique solution for θ can be found. This method can be augmented to be solved iteratively online for $y_k = \phi_k^{\mathrm{T}} \theta_k + \bar{\epsilon}_k$ leading to the recursive least squares (RLS) method defined by

$$\begin{aligned} L_k &= \frac{P_{k-1} \phi_k}{\lambda + \phi_k^{\mathrm{T}} P_{k-1} \phi_k}, \\ P_k &= \frac{1}{\lambda}(P_{k-1} - L_k \phi_k^{\mathrm{T}} P_{k-1}), \\ \theta_k &= \theta_{k-1} + L_k (F_k - \phi_k^{\mathrm{T}} \theta_{k-1}), \end{aligned}$$

when the weighting factor $\lambda = 1$. This method is well suited for constant parameters. However, since all information is held in the covariance matrix

$$P[k]^{-1} = \sum_{i=1}^{k} \phi\phi^{\mathrm{T}},$$

even if if the prediction error is nonzero, the parameter vector will not change. To allow for parameter changes the exponential weighting factor λ, also known as the forgetting factor, is used to discount old data and weight new data more heavily. Thus, when $0 < \lambda \leq 1$ is used the method is called exponentially weighted recursive least squares (EWRLS).

2.5.2 Kalman Filtering

The Kalman filter is an algorithm that estimates states assuming a Gaussian process for the system with a mean and covariance. An initial belief $\bar{x}$ based on the previous mean x_{k-1} and covariance $\bar{\Sigma}$ is update from the output $C(\bar{x}_k)$ or measurements $h(\bar{x}_k)$. The Kalman gain K, which weights how much of the measurement should be used to correct the initial belief is then calculated . The new belief and covariance x_k and Σ_k respectively, are the best solution in the least squared sense. The Kalman filter (KF) is implemented as follows

$$\begin{aligned}
\bar{x}_k &= A_k x_{k-1} + B_k u_k, \\
\bar{\Sigma}_k &= A_k \Sigma_{k-1} A_k^{\mathrm{T}} + R_k, \\
K_k &= \bar{\Sigma}_k C_k^{\mathrm{T}} (C_k \bar{\Sigma}_k C_k^{\mathrm{T}} + Q_k)^{-1}, \\
x_k &= \bar{x}_k + K_k[z_k - C(\bar{x}_k)], \\
\Sigma_k &= (I - K_k C_k)\bar{\Sigma}_k,
\end{aligned}$$

where A is the state transition matrix, B is the control input matrix and C is the output or observation matrix.

Extended Kalman Filter

The extended Kalman filter (EKF) uses a Taylor series linearization to handle nonlinear function that are not Gaussian. This allows for the augmentation of the state vector to include simultaneous parameter estimation. However, since the state transition G and observation H are linearized as Jacobians, the solution is no longer optimal.

The EKF algorithm can be implemented as follows

$$
\begin{aligned}
\bar{x}_k &= f(u_k, x_{k-1}), \\
\bar{\Sigma}_k &= G_k \Sigma_{k-1} G_k^{\mathrm{T}} + R_k, \\
K_k &= \bar{\Sigma}_k H_k^{\mathrm{T}} (H_k \bar{\Sigma}_k H_k^{\mathrm{T}} + Q_k)^{-1}, \\
x_k &= \bar{x}_k + K_k[z_k - h(\bar{x}_k)], \\
\Sigma_k &= (I - K_k H_k)\bar{\Sigma}_k,
\end{aligned}
$$

where

$$
G = \left.\frac{\partial f}{\partial x}\right|_{x_k}, \quad H = \left.\frac{\partial h}{\partial x}\right|_{x_k},
$$

and I is an identity matrix, $f(u, x)$ is the nonlinear state probability equation, R is the process covariance, and Q is the measurement covariance.

Uncented Kalman Filter

The unscented Kalman filter (UKF) is a variation of the Kalman filter that uses a different linearization method involving a weighted linear regression process. This is done by the use of sigma points χ. Given n states, there are $2n + 1$ sigma points defined by

$$
\begin{aligned}
\chi[0] &= \mu, \\
\chi[i] &= \mu + (\sqrt{(n+\lambda)\Sigma})_i, \quad i = 1, \ldots, n, \\
\chi[i] &= \mu - (\sqrt{(n+\lambda)\Sigma})_{i-n}, \quad i = n+1, \ldots, 2n,
\end{aligned}
$$

where μ is the mean, Σ is the covariance; $\lambda = \alpha^2(n + \kappa) - n$, where α and κ are scaling factors for the sigma points' separation from the mean. Two weights are assigned to the sigma points as

$$
\begin{aligned}
w_m[0] &= \frac{\lambda}{n+\lambda}, \\
w_c[0] &= \frac{\lambda}{n+\lambda} + (1 - \alpha^2 + \beta), \\
w_m[i] &= w_c[i] = \frac{1}{2(n+\lambda)}, \quad i = 1, \ldots, 2n,
\end{aligned}
$$

where β is used for the distribution with $\beta = 2$ for a true Gaussian.

The UKF algorithm can be implemented as follows

$$
\begin{aligned}
\chi_{k-1} &= (\mu,\ \mu + \sqrt{(n+\lambda)\Sigma_{k-1}},\ \mu - \sqrt{(n+\lambda)\Sigma_{k-1}}),\\
\chi_k^* &= f(u_k, \chi_{k-1}),\\
\bar{\mu}_k &= \sum_{k=0}^{2n} w_m[i]\chi_k^*[i],\\
\bar{\Sigma} &= \sum_{k=0}^{2n} w_c[i](\chi_k^*[i] - \bar{\mu}_k)(\chi_k^*[i] - \bar{\mu}_k)^{\mathrm{T}} + R_k,\\
\chi_k &= (\bar{\mu},\ \bar{\mu} + \sqrt{(n+\lambda)\bar{\Sigma}_k},\ \bar{\mu} - \sqrt{(n+\lambda)\bar{\Sigma}_k}\ ),\\
Z_k &= h(\chi_k),\\
\hat{z}_k &= \sum_{k=0}^{2n} w_m[i]Z_k[i],\\
S_k &= \sum_{k=0}^{2n} w_c[i](Z_k[i] - \hat{z}_k)(Z_k[i] - \hat{z}_k)^{\mathrm{T}},\\
\Sigma_k^{x,z} &= \sum_{k=0}^{2n} w_c[i](\chi_k[i] - \bar{\mu}_k)(Z_k[i] - \hat{z}_k)^{\mathrm{T}},\\
K_k &= \Sigma_k^{x,z} S_k^{-1},\\
\mu_k &= \bar{\mu} + K_k(z_k - \hat{z}_k),\\
\Sigma_k &= \bar{\Sigma}_k - K_k S_k K_k^{\mathrm{T}}.
\end{aligned}
$$

2.6 Backstepping Control with Parameter Estimation

As a different approach to the estimation methods outlined above, Lyapunov based adaptive parameter estimation can be used to provide control as well as parameter update laws. One way of implementing this is through the use of adaptive backstepping for nonlinear tracking in the presence of unknown parameters. Provided that the system in question has matched structure, i.e. the control term is in the span of the terms containing unknown parameters, a controller is first designed implementing adaptive backstepping assuming known parameters. Utilizing certainty-equivalence, the unknown parameters are then replaced by their estimates, and substituted into the dynamics equation. This yields the error system. The update law for the parameter estimate is then obtained via Lyapunov function consisting of the system and parameter error.

The generalized design process is outlined as follows. Consider a nonlinear system that can

be written in parametric strict feedback form

$$\begin{aligned}\dot{x}_i &= x_{i+1} + \varphi_i(x_1, \ldots, x_i)^{\mathrm{T}}\theta, \quad i = 1, \ldots, n-1,\\ \dot{x}_n &= \beta(x)u + \varphi_n(x)^{\mathrm{T}}\theta,\end{aligned} \tag{2.4}$$

with the output $y = x_1$ and where $\theta \in \mathbb{R}^p$ is the vector of unknown parameters, $\varphi = [\varphi_1, \ldots, \varphi_] \in \mathbb{R}^n$ is a vector of smooth functions whose components are in $\mathbb{R}^p$, $\beta(x) \neq 0\ \forall x \in \mathbb{R}^n$. It is desired for (2.4) to asymptotically track a trajectory of a reference model given by

$$\begin{aligned}\dot{x}_{\mathrm{r}} &= \begin{bmatrix} 0 & & \\ \vdots & & I_{n-1} \\ 0 & & \\ -m_0 & \cdots & -m_{n-1} \end{bmatrix} x_{\mathrm{r}} + \begin{bmatrix} 0 \\ \vdots \\ 0 \\ k_m \end{bmatrix} r,\\ y_{\mathrm{r}} &= x_{\mathrm{r},1},\end{aligned}$$

where the state matrix is Hurwitz, $k_m > 0$, and $r(t)$ is a bounded and piecewise continuous reference input where the derivatives of y_{r} are available from the states, $y_{\mathrm{r}}^i = x_{r,i+1}$. Using backstepping, the adaptive nonlinear controller can be recursively obtained as follows

$$\begin{aligned}z_i =& x_i - y_{\mathrm{r}}^{i-1} - \alpha_{i-1},\\ \alpha_i =& -z_{i-1} - c_i z_i - w_i^{\mathrm{T}}\hat{\theta} + \sum_{k=1}^{i-1}\left(\frac{\partial \alpha_{i-1}}{\partial x_k}x_{k+1} + \frac{\partial \alpha_{i-1}}{\partial y_r^{k-1}}y_{\mathrm{r}}^k\right)\\ & - d_i z_i + \frac{\partial \alpha_{i-1}}{\partial \hat{\theta}}\Gamma\tau_i + \sum_{k=2}^{i-1}\frac{\partial \alpha_{k-1}}{\partial \hat{\theta}}\Gamma w_i z_k,\\ \tau_i =& \tau_{i-1} + w_i z_i,\\ w_i =& \varphi_i - \sum_{k=1}^{i-1}\frac{\partial \alpha_{i-1}}{\partial x_k}\varphi_k,\end{aligned} \tag{2.5}$$

where $c_i > 0,\ i = 1, \ldots, n,\ z_0 \triangleq 0,\ \alpha_0 \triangleq 0,\ \tau_0 \triangleq 0$. This leads to the control law

$$u = \frac{1}{\beta(x)}[\alpha_n + y_{\mathrm{r}}^n],$$

making the error system $\dot{z} = A_z(z, \hat{\theta}, t)z + W(z, \hat{\theta}, t)^{\mathrm{T}}\tilde{\theta},\ z \in \mathbb{R}^n$ where $z_1 = x_1 - x_{\mathrm{r},1} = y - y_{\mathrm{r}}$ is the tracking error, and the matrix-valued functions A_z and W are

$$A_z(z,\hat{\theta},t) = \begin{bmatrix} -c_1 - d & 1 & 0 & \dots & 0 \\ -1 & -c_2 - d & 1+\sigma_{23} & \cdots & \sigma_{2n} \\ 0 & -1-\sigma_{23} & \ddots & \ddots & \vdots \\ \vdots & \vdots & \ddots & \ddots & 1+\sigma_{n-1,n} \\ 0 & -\sigma_{2n} & \cdots & -1-\sigma_{n-1,n} & -c_n - d \end{bmatrix},$$

$$W(z,\hat{\theta},t) = \begin{bmatrix} w_1, & \dots, & w_n \end{bmatrix} \in \mathbb{R}^{p\times n},$$

where $\sigma_{ik} = -\frac{\partial \alpha_{i-1}}{\partial \hat{\theta}}$. In the above controller design, $d = \kappa_i |w_i|^2$ is an optional nonlinear damping factor that improves the transient response of the system, but may be omitted if desired. Choosing the Lyapunov function as

$$V = \frac{1}{2} z^{\mathrm{T}} z + \frac{1}{2} \tilde{\theta}^{\mathrm{T}} \Gamma^{-1} \tilde{\theta},$$

leads to the update law

$$\dot{\hat{\theta}} = \Gamma W z.$$

For further detail on the derivation of the above design, the reader is referred to [72].

2.7 Nonlinear Swapping

Nonlinear swapping provides a method to deal with unknown time varying parameter estimates by using filters. Consider the nonlinear system

$$\begin{aligned} \dot{z} &= A_z(z,\hat{\theta},t) z + W(z,\hat{\theta},t)^{\mathrm{T}} \tilde{\theta} + D(z,\hat{\theta},t)^{\mathrm{T}} \dot{\hat{\theta}}, \\ y_1 &= h(z,\hat{\theta},t) z + l(z,\hat{\theta},t) W(z,\hat{\theta},t)^{\mathrm{T}} \tilde{\theta}, \end{aligned} \tag{2.6}$$

along with the filters

$$\begin{aligned} \dot{\Omega}^{\mathrm{T}} &= A(z,\hat{\theta},t)\Omega^{\mathrm{T}} + g(z,\hat{\theta},t) W(z,\hat{\theta},t)^{\mathrm{T}}, \\ y_2 &= h(z,\hat{\theta},t)\Omega^{\mathrm{T}} + l(z,\hat{\theta},t) W(z,\hat{\theta},t)^{\mathrm{T}}, \end{aligned} \tag{2.7}$$

$$\begin{aligned} \dot{\psi} &= A(z,\hat{\theta},t)\psi + \Omega^{\mathrm{T}} \dot{\tilde{\theta}} + Q(z,\hat{\theta},t)^{\mathrm{T}} \dot{\tilde{\theta}}, \\ y_3 &= -h(z,\hat{\theta},t)\psi. \end{aligned} \tag{2.8}$$

Assuming that z is continuous on $[0,\infty]$ and that there exists a continuously differentiable function $V:\mathbb{R}^n\times\mathbb{R}_+\to\mathbb{R}_+$ such that

$$\alpha_1|\zeta|^2\le V(\zeta,t)\le\alpha_2|\zeta|^2, \tag{2.9}$$

and for each $z\in C^0$,

$$\frac{\partial V}{\partial\zeta}A(z,\hat{\theta},t)\zeta+\frac{\partial V}{\partial t}\le-\alpha_3|\zeta|^2, \tag{2.10}$$

$\forall t\ge 0,\ \forall\zeta\in\mathbb{R}^n;\ \alpha_1,\ \alpha_2,\ \alpha_3>0$, then $\forall z(0),\ \phi(0)\in\mathbb{R}^n,\forall\Omega(0)\in\mathbb{R}^{p\times n},\ \forall t\ge 0$ the outputs of (2.6) - (2.8) are related by

$$y_1=y_2\tilde{\theta}+y_3+y_\epsilon.$$

Noting that

$$\begin{aligned}y_\epsilon(t)&=y_1-y_3-y_2\tilde{\theta}\\&=hz+h\psi+lW^{\mathrm{T}}\tilde{\theta}-h\Omega\\&=h(z+\phi-\Omega^{\mathrm{T}}\tilde{\theta})\\&=h(z,\hat{\theta},t)\tilde{\epsilon},\end{aligned}$$

and differentiating $\tilde{\epsilon}=z+\phi-\Omega^{\mathrm{T}}\tilde{\theta}$ we obtain

$$\begin{aligned}\dot{\tilde{\epsilon}}&=\dot{z}+\dot{\psi}-\dot{\Omega}^{\mathrm{T}}\tilde{\theta}-\Omega^{\mathrm{T}}\dot{\tilde{\theta}}\\&=A(z+\phi-\Omega^{\mathrm{T}}\tilde{\theta})\\&=A(z,\hat{\theta},t)\tilde{\epsilon},\end{aligned}$$

which used with (2.9) and (2.10) gives

$$\dot{V}(\tilde{\epsilon},t)=\frac{\partial V}{\partial\tilde{\epsilon}}A(z,\hat{\theta},t)\tilde{\epsilon}+\frac{\partial V}{\partial t}\le-\alpha_3|\tilde{\epsilon}|^2\le-\frac{\alpha_3}{\alpha_2}V.$$

Thus, V is uniformly bounded and $V(t)\to 0$ as $t\to 0$. Furthermore, $|\tilde{\epsilon}(t)|\le\sqrt{V(t)/\alpha_1}$, implying that $\tilde{\epsilon}$ is uniformly bounded and converges to zero. Therefore, since $h(z,\hat{\theta},t)$ is bounded, y_ϵ is bounded and converges to zero.

2.8 Guaranteed Adaptive Parameter Estimation with Data Accumulation

Normally parameter estimation, whether derived through filtering or Lyapunov methods, requires persistent excitation. As a result, depending on the system convergence may not be achieved or it may be slow. To overcome the persistent excitation requirement the work in [35] utilizes nonlinear swapping to modify the Lyapunov function used to derive the parameter update laws. This is done by implementing stable data accumulation to ensure that the Lyapunov function is negative definite with respect to the parameter error, thereby guaranteeing convergence. This method is detailed here as follows.

Considering a system of the form $\dot{x} = f(x,u) + G(x,u)\theta$ with output $y_1 = h(x)x$, it is assumed that there exists a bound control law $u = \alpha(x,\hat{\theta},t)$ and an estimation law of the form $\dot{\hat{\theta}} = \Gamma_\theta \beta(z,x,\hat{\theta},t)$, that results in the closed loop error dynamics $\dot{z} = f(z,\hat{\theta},t) + G(z,\hat{\theta},t)\tilde{\theta}$, from a Lyapunov function of the form $V(z,\tilde{\theta} = z^{\mathrm{T}}z + \tilde{\theta}^{\mathrm{T}}\Gamma_\theta^{\mathrm{T}}\tilde{\theta}$, whose derivative is $\dot{V} = -z^{\mathrm{T}}Cz$, where $\tilde{\theta} = \theta - \hat{\theta}$, and C is positive definite. The estimation law is modified as

$$\dot{\hat{\theta}} = \Gamma_\theta(\beta + \mu),$$

where

$$\mu = M\tilde{\theta} = W_x^{\mathrm{T}}\Gamma_x\varsigma_x + Q^{\mathrm{T}}\Gamma_\psi\tilde{\psi},$$

such that the Lyapunov derivative becomes

$$\dot{V} = -z^{\mathrm{T}}Cz - \tilde{\theta}^{\mathrm{T}}M\tilde{\theta}. \tag{2.11}$$

If M is positive definite, the Lyapunov derivative is negative definite and the estimation error converges to zero according to the LaSalle-Yoshizawa theorem [72].

To make M positive definite, nonlinear swapping and data accumulation is implemented as follows. First, an algebraic connection between the system states and the parameters is made using the filters for nonlinear swapping as

$$\dot{\hat{x}} = -\Lambda_x(x - \hat{x}) + f + G\hat{\theta} + K_x^{-1}W_x\dot{\hat{\theta}}, \quad y_2 = h(\hat{x})\hat{x}, \tag{2.12}$$

$$\dot{W}_x = \Lambda_x W_x + K_x G, \quad y_3 = h(x)K_x^{-1}W_x, \tag{2.13}$$

such that

$$\dot{\tilde{\epsilon}} = \Lambda_x\tilde{\epsilon},$$

where $W_x \in \mathbb{R}^{n\times p}$, $\tilde{\epsilon} \in \mathbb{R}^{n\times 1}$, and the tuning matrices $K_x = \mathrm{diag}(k_{x_1},\ldots,k_{x_n})$ $\Lambda_x = \mathrm{diag}(\lambda_{x_1},\ldots,\lambda_{x_n})$ are positive definite and negative definite respectively. All signals are globally bounded and $W_x\tilde{\theta} = \varsigma_x$ with the relation $\varsigma_x = K_x(e_x - \tilde{\epsilon})$.

Proof. From the choice of filters, the outputs are related by

$$y_\epsilon = h(x)\tilde{\epsilon} = y_1 - y_2 - y_3\tilde{\theta},$$

such that

$$\tilde{\epsilon} = x - \hat{x} - K_x^{-1}W_x\tilde{\theta}.$$

Differentiating and substituting

$$\begin{aligned}
\dot{\tilde{\epsilon}} &= \dot{x} - \dot{\hat{x}} - K_x^{-1}\dot{W}_x\tilde{\theta} - K_x^{-1}W_x\dot{\tilde{\theta}} \\
&= f + G\theta - (-\Lambda_x(x-\hat{x}) + f + G\hat{\theta} + K_x^{-1}W_x\dot{\hat{\theta}}) - K^{-1}(\Lambda_x W_x + K_x G)\tilde{\theta} - K_x^{-1}W_x\dot{\tilde{\theta}} \\
&= \Lambda_x(x-\hat{x}) - K_x^{-1}W_x\tilde{\theta} - K_x^{-1}W_x\dot{\tilde{\theta}} - K_x^{-1}W_x\dot{\hat{\theta}} \\
&= \Lambda_x(x - \hat{x} - K_x^{-1}W_x\tilde{\theta}), \\
\dot{\tilde{\epsilon}} &= \Lambda_x\tilde{\epsilon}.
\end{aligned}$$

Furthermore, the relation given by ς_x is confirmed by substituting in $\tilde{\epsilon}$ into $\varsigma_x = K_x(e_x - \tilde{\epsilon})$,

$$\begin{aligned}
W_x\tilde{\theta} = \varsigma_x &= K_x(e - \tilde{\epsilon}) \\
&= K_x((x-\hat{x}) - (x - \hat{x} - K_x^{-1}W_x\tilde{\theta})) \\
&= K_x K_x^{-1}W_x\tilde{\theta}, \\
W_x\tilde{\theta} &= W_x\tilde{\theta}.
\end{aligned}$$

□

Next, a coordinate transform $\psi = Q\theta$ is performed for data accumulation such that

$$\begin{aligned}
\dot{Q} &= \Lambda_r(Q_r - Q)W_x^{\mathrm{T}}R_xW_x, \quad Q(0) = 0, \\
\dot{\psi} &= -\Lambda_r(Q_r - Q)W_x^{\mathrm{T}}R_x(\varsigma_x + W_x\hat{\theta}), \quad \psi(0) = 0, \\
\hat{\psi} &= Q\hat{\theta},
\end{aligned}$$

where R_x is positive definite, Λ_r is negative definite, Q_r is a constant full rank reference matrix, and $\tilde{\psi} = \psi - \hat{\psi} = Q\tilde{\theta}$.

The definition of these signals through nonlinear swapping and data accumulation is done such that $\tilde{\psi}$ converges to zero and Q achieves full rank, so that the estimation error $\tilde{\theta}$ converges to zero. This is evident given when Q has full rank, $M = W_x^{\mathrm{T}}\Gamma_x\varsigma_x + Q^{\mathrm{T}}\Gamma_\psi Q$ has full rank and is positive definite, making eqn. (2.11) negative definite and guaranteeing the parameter error converges to zero.

Chapter 3

Using an SEA to Extend Performance in Time Delays

D. Budolak and P. Ben-Tzvi, "Series elastic actuation for improved transparency in time delayed haptic teleoperation,"*Mechatronics*, vol. 63, p. 102278, 11 2019 [73].

Mechanical aspects of the teleoperation system have often been overlooked as possible avenues to address system performance. Previously, researchers have focused primarily on control methods for the communication channel to improve performance and system passivity. In a different approach to the problem, this work proposes the novel use of an SEA as a compliant end effector for the follower side. The addition of an SEA for passive compliance on the follower provides many advantages for improving the capabilities of teleoperation systems. These advantages are discussed in detail in the following sections.

3.1 Proposed System

The proposed system uses an F-P architecture with a predictive control strategy to combat the effects of time delay. In this approach, the remote robot tracks a position command from the master device and sends back the external force from the environment. The environmental force is then reflected back onto the user by the master haptic device. Because the remote side tracks the master position it will be referred to as the follower. In this scheme, transparency is achieved through position and force matching such that $x_{\mathrm{h}} = x_{\mathrm{e}}$ and $F_{\mathrm{h}} = F_{\mathrm{e}}$, where the subscripts h and e refer to the human operator and environment respectively. For the predictive control, a Smith predictor (SP) is used. With this approach, the delayed force from the follower-environment interaction is cancelled out by the predictive model. However, the controller must have perfect knowledge of the delay and entire follower side dynamics. Any modeling error will result in degraded system performance and potential instability. Because the delay is cancelled out, the user on the master side will receive feedback from the system as if there is no delay. The block diagram for this proposed architecture is depicted in Fig. 3.1.

For the SEA in the proposed system, a generalized force sensing rotary model, similar to that

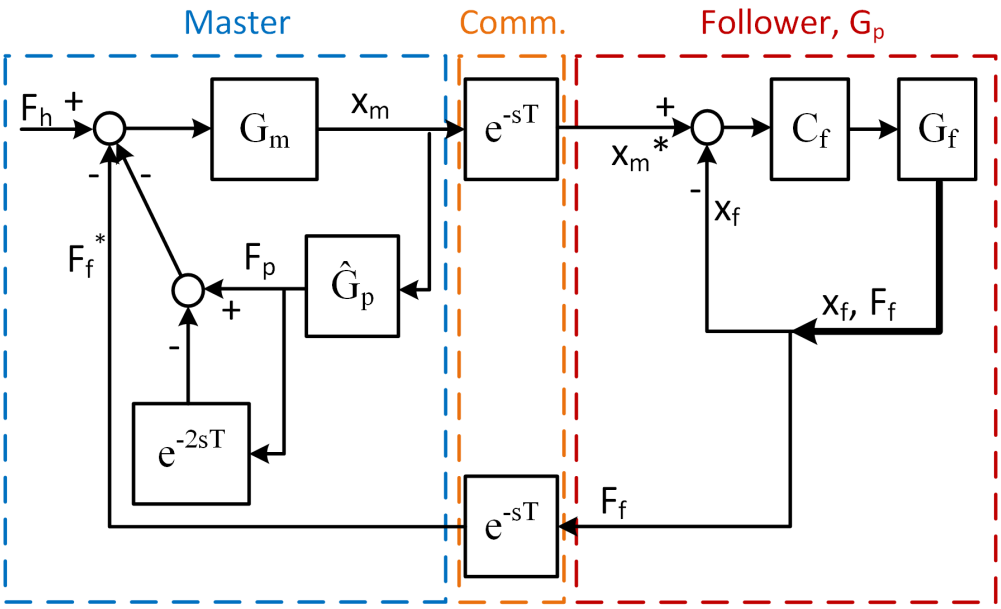

Figure 3.1: Block diagram of the proposed force-position Smith predictor architecture.

examined by [74], is formulated and modified for a linear case. Including the electrical and mechanical subsystems, the SEA is modeled as follows. The electrical system is coupled to the motor dynamics by the motor torque, which is proportional to the current as $\tau_{\mathrm{m}} = K_{\mathrm{m}} i$ with motor constant K_{m}. The motor is coupled to the load by τ_{out} through the spring displacement $d_{\mathrm{s}} = N^{-1}\theta_{\mathrm{m}} - \theta_l$, giving

$$\begin{aligned} Ri + L\tfrac{di}{dt} + K_{\mathrm{m}}\dot{\theta}_{\mathrm{m}} &= V, \\ J_{\mathrm{m}}\ddot{\theta}_{\mathrm{m}} + B_{\mathrm{m}}\dot{\theta}_{\mathrm{m}} &= \tau_{\mathrm{m}} - \tau_{\mathrm{out}}, \\ J_l\ddot{x}_l + B_l\dot{x}_l &= \tau_{\mathrm{out}} + \tau_{\mathrm{ext}}, \\ K_{\mathrm{s}} d_{\mathrm{s}} &= \tau_{\mathrm{out}}, \end{aligned} \tag{3.1}$$

where J_l and B_l are the mass and damping of the load, J_{m} and B_{m} are the motor inertia and damping, V is the voltage applied to the motor, L is the armature inductance, and R is the armature resistance.

For the proposed linear actuator, the rotary motion from the DC motor is converted into linear motion with a lead screw as $x_{\mathrm{m}} = N^{-1}\theta_{\mathrm{m}} l/2\pi$, where l is the screw pitch. The force applied by the SEA is then $F_{\mathrm{out}} = K_{\mathrm{s}} d$ where displacement $d = x_{\mathrm{m}} - x_l$, and x_{m} and x_l are the motor and load positions. The general linear load dynamics now become $M_l\ddot{x}_l + B_l\dot{x}_l = F_{\mathrm{out}} + F_{\mathrm{ext}}$.

From the system of equations above, an open loop transfer function relating the output force

of the SEA to the input voltage while the follower is in contact can be written as

$$\frac{F_{\text{out}}}{V} = \frac{K_{\text{s}} K_{\text{m}} l}{2\pi s[(Ls+R)(J_{\text{m}}s + B_{\text{m}}) + K_{\text{m}}^2]}.$$

A PID control law can now be applied to this for position control of the SEA for implementation of the proposed F-P architecture as follows

$$e = x_{\text{m}} - x_{\text{f}},$$
$$V = K_{\text{P}} e + K_{\text{I}} \int e + K_{\text{D}} \dot{e}.$$

Without loss of generality, x_{f} can be set to zero with x_{m} being the new set point relative to x_{f}. The transfer function for the follower side dynamics for use in calculating F_{p} in the SP is now

$$G_{\text{p}} = \frac{K_{\text{s}} K_{\text{m}} l(K_{\text{D}} s^2 + K_{\text{P}} s + K_{\text{I}})}{2\pi s^2[(Ls+R)(J_{\text{m}}s + B_{\text{m}}) + K_{\text{m}}^2]}.$$

3.2 Advantages of Compliance in the System

The addition of passive compliance to the follower provides many advantages for improving the capabilities of teleoperation systems. In the implementation of an F-P architecture, the reflected force becomes proportional to the follower position through the spring constant. Therefore the outer loop force control also drives the position tracking. In this manner, the transperency of the position and force are coupled and no longer subject to the same drift due to the performance-stability trade off. In addition to reducing the common deviation between force and position error, the compliance also simplifies modeling of the follower-environment with favorable contact conditions. Because an SEA duels as a sensor and actuator, it also provides a convenient sensing method for the environment contact pint, allowing to adjust for movement of the environment. Moreover, the SEA helps to decouple the inertia of links in a manipulator, reducing impact forces that can help the contact in many applications. Overall, due to the compliance and force position relationship, the system is far more robust, in particular in the presence of large time delays.

3.2.1 Simplification in Environment Force Modeling

Compliance is beneficial because with two objects in contact, the kinematics of the most compliant member dominates. This becomes evident by examining the pole locations of both a stiff and compliant system. The time constant depends on the pole locations $\text{Re}\{\lambda\}$, where λ is an eigenvalue of the system. λ's with large time constants decay quickly and only the compliant dynamics remain. Thus, if the follower has a compliant member such as an SEA in

contact with the environment, where the follower impedance is much smaller than that of the environment, $Z_\mathrm{f} \ll Z_\mathrm{e}$, then the force exerted by the follower on the environment reduces to the SEA spring displacement as given by Hooke's Law. However, this simplification cannot be made with a stiff follower, or when the compliances have a similar relative order of magnitude. For these cases the environmental force can be expressed as

$$F_\mathrm{e} = \begin{cases} -K_\mathrm{s}(x_\mathrm{e} - x_\mathrm{f}), & K_\mathrm{f} \ll K_\mathrm{e} \\ f(x_\mathrm{f}, x_\mathrm{e}, \dot{x}_\mathrm{e}), & K_\mathrm{f} \gg K_\mathrm{e}, K_\mathrm{f} \approx K_\mathrm{e}, \end{cases}$$

where K is stiffness with subscripts e, f, and s referring to the follower, environment, and SEA respectively. f is a generalized function that is dependent on the follower position x_f, environment contact location x_e, velocity $\dot{x}_\mathrm{e}$, and may be time-varying with linear or nonlinear stiffness and damping. Naturally, if $K_\mathrm{f} \gg K_\mathrm{e}$ then the SEA will be unable to measure the contact force since the spring does not displace. For measuring environmental forces in this situation, a secondary force sensor can be used at the expense of stiff contact behavior common in F-P architectures. Thus, the spring stiffness must be appropriately selected for the environment and use case. Environment dynamics can also be nonlinear. With traditional SP approaches, nonlinear environment dynamics cause prediction errors that lead to transparency losses, thereby destabilizing the system. With an SEA, the environment position is known through contact with the follower and the position is encoded in the force signal. This is used to update the prediction model and allows the proposed system to have good force and position tracking even in contact with soft nonlinear environments.

3.2.2 Environment Contact Location Sensing and Correction

Compensating for time varying environment dynamics is important for teleoperation systems with large time delays since prediction schemes in particular necessitate exact knowledge of the follower and environment dynamics. Generally, the follower side dynamics are assumed to be known a priori and not subject to disturbances. In predictive architectures, inaccurate estimation will have losses in transparency from delay cancellations, and subsequently large force reflection error. Thus, any unknown environmental variations can lead to undesired collisions resulting in destabilizing oscillations or damage to the system and environment. Because the SEA is capable of both position and force sensing, it can be used to compensate for varying environment dynamics without the use of a neural network or an adaptive control scheme. For environment position variation, if there is an error in the environment contact location, $F_\mathrm{p} \neq F_\mathrm{f}$ even if $x_\mathrm{m} = x_\mathrm{f}$. Because the force on the follower is proportional to the SEA spring displacement, x_e can be calculated by the difference in follower position and spring displacement as

$$x_\mathrm{e} = x_\mathrm{f} - \frac{F_\mathrm{f}}{k_\mathrm{s}}. \tag{3.2}$$

The spring displacement cannot be used directly since the F-P architecture only uses two channels to send and receive the position and force respectively. During operation when the environment position varies, the contact location x_e is determined from eqn. (3.2) upon initial contact with the environment, and the force reflection is carried out with the new estimate. This method continuously updates x_e while in contact with the environment.

3.2.3 Simulation for Contact with Hard and Soft Environments

Since the proposed solution involves compliant contact with the environment using an SEA, a simulation was performed to examine the advantages and consequences of such contact. Additionally, aspects of the follower side lower level control strategy were examined as a means to further investigate this application. As the simulation involves only the follower side, no delay was used for this simulation. The rationale behind such a simulation and looking into these cases is that as the literature review mentions, there has been little work done to explore these affects as they pertain to teleoperation. Often, the initial contact dynamics are not considered in teleoperation since a stationary environment is passive from energy and momentum conservation of impact. However, this ignores important aspects of the system such as the large impulses that occur due to discontinuity in velocity upon impact. When these are large, the resulting oscillations can degrade performance, in particular for higher speeds. Perhaps since teleoperation was developed with a "move and wait" strategy in its formative years [1], most studies and applications have been low bandwidth, which helps in the follower prediction but limits practical application. Another advantage of SEA's over direct drive actuators is that they do not have chatter when in contact from a stiff load cell reading in high gain feedback [38]. This is an important distinction further investigated in simulation, as this sensing method is implemented most often for teleoperation. Moreover, gain limitations affect the amount of modeling error the system can handle with an SP as discussed above.

To further investigate how the contact dynamics affect the system, a simulation was carried out in MATLAB for a generalized scenario of a 0.1 m rod making contact with a wall 0.05 m away. Actuation with a stiff motor was compared to a rotary force sensing SEA with dynamics defined by eqn. (3.1) with parameters listed in Table 3.1. Unilateral contact dynamics were implemented using the nonlinear Hunt-Crossley (HC) model [26].

Results for contact with a stiff environment are depicted in Fig. 3.2 for K_e and c_r values of 2.8×10^9 and 0.75 respectively, with a proportional gain K_P of 7.5. The target force was set to 2.5 N. The results show a substantial amount of chatter and overshoot for the stiff motor, whereas the SEA settles much faster within the acceptable error. The simulation was repeated for contact with a soft wall with K_e, c_r, and K_P values of 2.8×10^4, 0.5, and 18. As the wall stiffness decreases, the SEA loses its compliance advantage and has a larger settling time than the motor as demonstrated in Fig. 3.3. It should be noted that because of the compliance and damping of the material, the motor settles behind the nominal contact

location as the wall is deformed. Moreover, because of the SEA compliance the final settling distance within the wall is different despite having a negligible difference in steady state error.

In the proposed F-P architecture, the follower is position controlled. Simulations were also run for stiff and soft contact with proportional position control targeting the wall location at 0.05 m. The same K_{e} and c_{r} were used as before with K_{P} set to 80. Results did not vary much for stiff and soft contact, and are shown in Fig. 3.4. In both cases the stiff motor had large overshoot and chatter, but occurring with much less frequency than in the force control case. The SEA showed less overshoot than with force control. These results support the use of an SEA over a stiff motor for sensing and actuation as a means to increase the capabilities of delayed teleoperation systems.

Table 3.1: Simulation parameters.

Parameter	Value
J_{m}	4 E-6 Kg·m^2
J_l	2 E-4 Kg·m^2
B_{m}	2.9 E-5 Nm·s/rad
B_l	1.0 E-4 Nm·s/rad
K_{s}	5 Nm/rad
N	10
R	4 Ω
L	2.7 E-6 H
K_{m}	0.0275 Nm/$\sqrt{\mathrm{W}}$

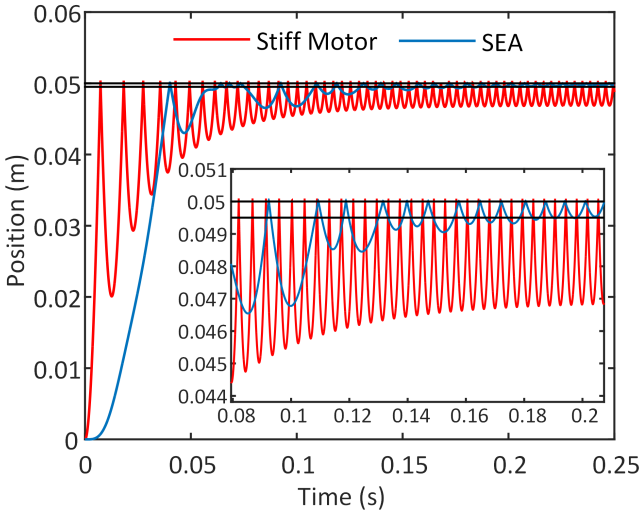

Figure 3.2: SEA vs. Stiff Motor simulation results in force control with stiff unilateral contact force modeling.

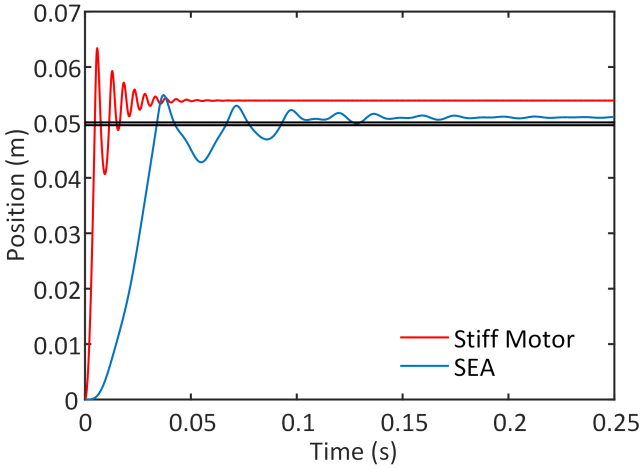

Figure 3.3: SEA vs. Stiff Motor simulation results in force control with soft unilateral contact force modeling.

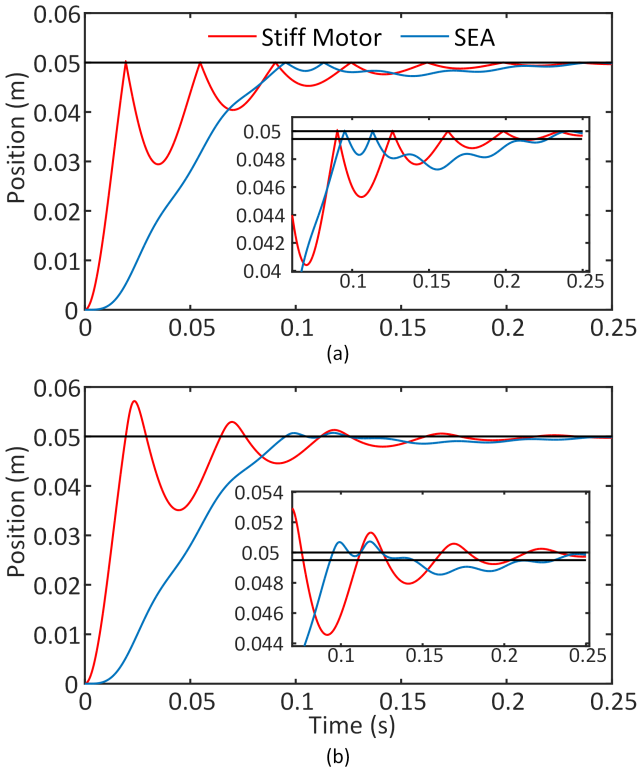

Figure 3.4: SEA vs. Stiff Motor simulation results in position control with (a) stiff and (b) soft unilateral contact force modeling.

3.3 Haptic Teleoperation Experiment

Experiments were set up to validate that the performance of a time delayed system is improved by the use of an SEA, as well as demonstrate the capability to adapt to a varying environment. A Geomagic Touch haptic device was used as the master and a force sensing SEA as the follower. The experimental setup is shown in Fig. 3.5. For the experiment, a one degree of freedom contact task was performed for ease of comparison with literature. The Geomagic Touch user input and haptic feedback was restricted to motion along one axis. The linear actuator on the follower side used a potentiometer for position feedback to implement the Smith predictor architecture from Fig. 3.1.

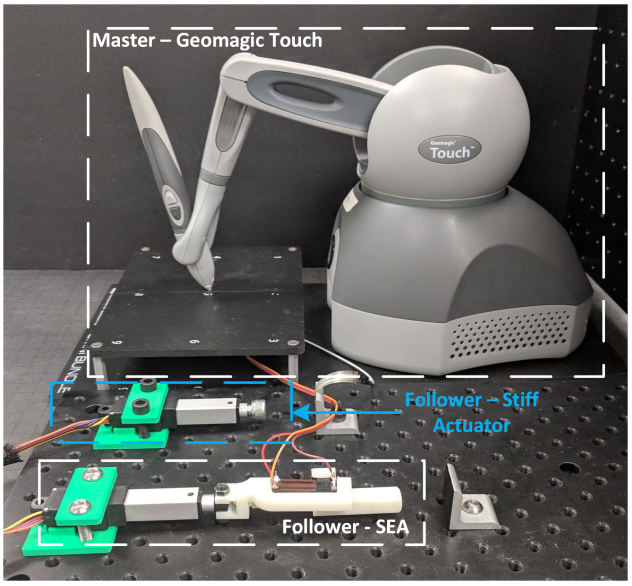

Figure 3.5: Experimental setup with Geomagic Touch, SEA, and stiff actuator.

The master side control was executed on a computer communicating through a serial port to a Teensy 3.2 microcontroller on the follower side. Although serial communication does not provide a constant delay, buffer sizes were set to achieve a maximum upper bound to the delay. The master side was implemented using Simulink, and a delay block was used to create a well controlled artificial delay. The Simulink model was executed at 1 kHz. The contact experiment was conducted for a 0.5, 1, and 2 s RTT. Contact with an aluminum wall was performed with a user input target force of around 2.5 N. The estimated force signal was displayed on the computer screen to aide the user. Contact was initiated for approximately two seconds and the device was returned to the starting position to repeat the contact. The experiment was conducted with an SEA in both a stationary and varying environment. A similar test was conducted for soft contact with foam.

The follower uses a Firgelli L12-30-210-6-P linear actuator with a guided compression spring and a 20 kOhm linear potentiometer for the spring displacement measurement. The spring

has an overall length of one inch and a stiffness of 0.86 N/mm (4.93 lbf/in). This size was chosen to investigate finer movements while staying within typical hand exoskeleton limits of 10 N [75]. The SEA was placed 9 mm from an aluminum L-bracket acting as the stiff wall. The environment contact position was known to the controller, and system identification was used to obtain a model for the SEA. A manually tuned PID controller was used on the follower to track the master position

3.3.1 SEA Hard Contact

From Fig. 3.6 it can be seen that the use of an SEA greatly increases performance in terms of transparency for position and force tracking. These results can be compared to existing work in the field that use a stiff follower as referenced in Section 2. One of the greatest benefits of this implementation is that accurate force matching is achieved without sacrificing position accuracy as with traditional methods. With the use of an SEA, position and force is linearly related and thus the follower position tracking is also part of the environment sensing and force reflection estimation. Consequently, any position errors from inaccurate modelling of the follower and environment dynamics will directly affect the force tracking. Additionally, from a more detailed inspection of Fig. 3.6, the resolution of the spring displacement affects the force reflection accuracy since the force and displacement are coupled in an SEA. However, the proposed system still demonstrates excellent performance, with force reflection accuracy to within a few tenths of a Newton, and position tracking to less than half a millimeter, even at a time delay of two seconds. Some data packet losses were observed, but the occurrence was infrequent and did not have any significant effects on performance.

Stiff Actuator Comparison

A similar experiment was carried out without compliance, using the same model linear actuator. A force sensing resistor (FSR) was placed on a stiff wall 6 mm away from the actuator end to sense the environment contact force as in a traditional F-P architecture. The FSR was calibrated by applying objects of varying weights to the sensor on a scale. The user made contact with the wall with a target applied force of 2.5 N as before. The results in Fig. 3.7 show the typical performance of such a system. At small time delays of 0.5 s, the force tracking is sufficiently accurate with significant position error typical in approaches using a stiff follower. As the time delay increases the force reflection performance diminishes.

3.3.2 Varying Environment and Soft Contact

In most studies, the environment is assumed to be stationary, and determining the contact location is often overlooked or assumed to be known a priori. This is one of the greatest

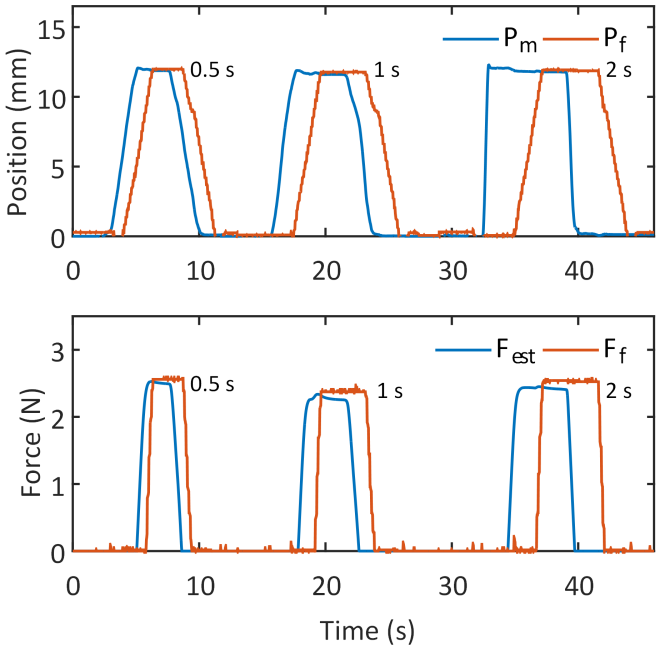

Figure 3.6: Master and follower contact with an aluminum bracket for a 0.5, 1, and 2 s RTT.

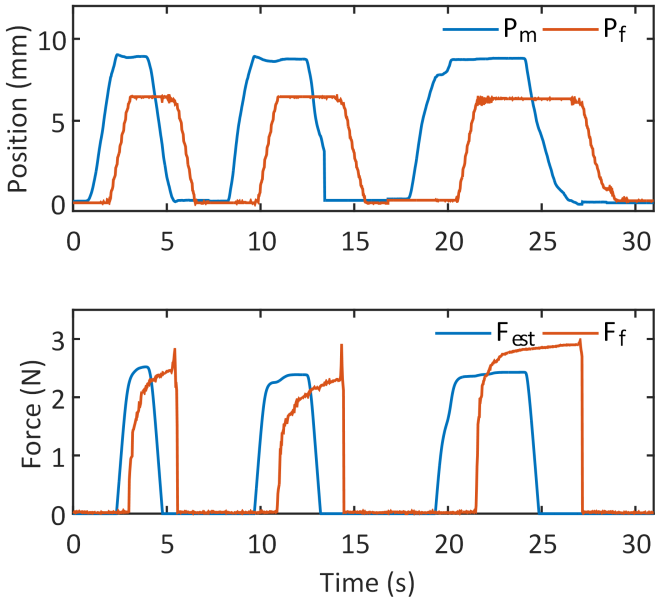

Figure 3.7: Master and stiff follower contact with aluminum bracket for 0.5, 1, and 2 s RTT.

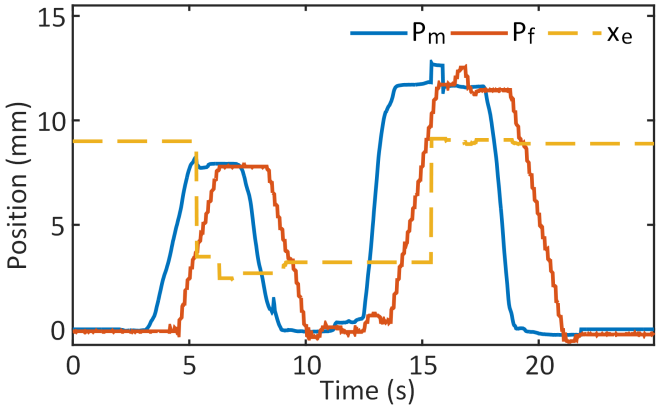

Figure 3.8: Example of master and follower position with a changing environment contact location in one second RTT.

Table 3.2: Varying environment contact location error.

RTT (s)	**3 mm Contact (mm)** max dev.	avg. settling dev.
0.5	0.688	0.336
1.0	0.647	0.393
2.0	0.534	0.522
RTT (s)	**9 mm Contact (mm)** max dev.	avg. settling dev.
0.5	0.186	0.102
1.0	0.209	0.097
2.0	0.094	0.102

limitations to practical application of teleoperation systems since environments in real life are often time varying. Based on a review of recent work, few studies have mentioned the capability to handle varying contact positions [15, 19], with limited discussion. However, the ability to adapt to time varying environments is important to extend the capabilities of teleoperation, particularly in the presence of time delay.

An experiment was conducted where the environment contact sensing and correction (ECSC) method defined in equation (3.2) was applied to the SEA controller. A 6 mm block was placed between the wall and the SEA to change the contact location. The user was instructed to make contact with the wall as before, assuming the original contact location at 9 mm. The teleoperation system was set with an initial contact location of 9 mm as well. After the first contact, the block was removed and the user was instructed to make a second contact at the original wall location at 9 mm. The ECSC is an online correction method that is constantly executed throughout the motion. However, because it is based on F_f, it is only updated once contact is initiated. Moreover, since the ECSC is on the follower side, the

user receives an update only after the backwards time delay duration, or half the RTT for a constant and symmetric delay as in this implementation. The accuracy of the sensing method is affected by the model accuracy and position error. As before, the SEA spring displacement resolution also has an effect on the ECSC and thus an appropriate sensor must be selected for the specific application of the teleoperation system.

Knowledge of the contact location is necessary for predictive approaches based on an SP, and affects the force sensing of the SEA. As such, this becomes critical information for the proposed teleoperation architecture. To evaluate the performance of the ECSC the test was conducted with five trials at RTT's of 0.5, 1, and 2 s. The maximum deviation and average settled value after contact is shown in table 3.2. The results do not follow any significant trend, although the average settled x_e error was larger for trials with a two second time delay. This is likely due to the increasing error between F_f and F_p as the communication delay increases, causing drift between the estimated x_e and the actual contact location. This provides the first quantitative result known to the authors for capabilities to compensate for environment variations. Contact tests were also conducted with a soft environment using

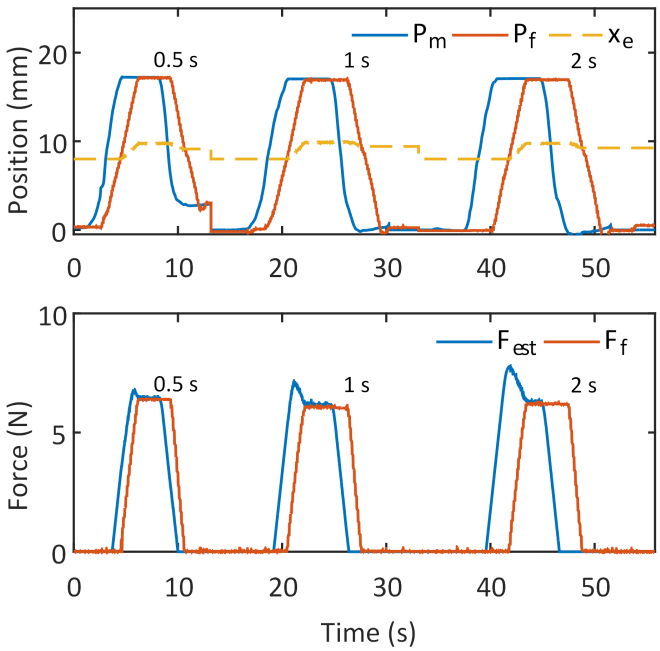

Figure 3.9: Master and follower contact with foam block environment location, 0.5, 1, and 2 s RTT.

a foam block. For soft materials the contact location changes as the material deforms. Therefore, x_e must be updated on the master side to prevent modelling errors that will degrade performance and potentially destabilize the system. Fig. 3.9 demonstrates the performance of the proposed system and the ability of the ECSC to correct for dynamic

environment variations on top of the static case discussed above.

For small time delays, the ECSC is able to correct $\hat{G}_{\mathrm{p}}$ with small force errors. As the delay increases, the update time causes greater force estimation overshoot until contact is maintained and the correction allows F_{est} and F_{f} to converge. Although in dynamic environment variation the correction will always trail the actual contact location, in small delays the performance can be acceptable for small bandwidths. Moreover, these results are particularly promising as the ECSC assumes no knowledge of the environment dynamics.

3.4 Conclusion

This work presented the improvement in performance and transparency for a robust teleoperation system with the use of an SEA on the follower side in a F-P architecture using a Smith predictor. Simulation results demonstrate the benefit of using an SEA for unilateral contact with a stiff environment over direct actuation. Compliance in the system demonstrated a reduction in chatter and overshoot for both force and position control in stiff and soft environments. In experiment, accurate force and position tracking was achieved in an RTT of two seconds for contact with a stiff environment. Additionally, a method to account for variations in contact location, ECSC, was developed and demonstrated. Contact with a soft environment showed good performance in an RTT delay of 500 ms, but diminished as the delay increased from modeling error of the soft environment.

Chapter 4

Online Estimation of Environment Dynamics for Model Based Methods

As indicated by the above results for the teleoperation system utilizing an SEA, contact with a soft environment requires better knowledge of the environmental contact force. This limitation can be addressed by using a better model of the environment in the predictive control scheme that can more accurately represent the interaction force with soft materials. In this proposed approach, parameters of the environment model are estimated online on the remote side and then sent to update the predictor on the master side of the teleoperation system. In this work, the Hunt-Crossley model is implemented as it the most widely used continuous contact model, with the ability to account for nonlinear stiffness and visco-elastic damping. A detailed definition and discussion of the HC model is presented in Section 2.2.

For the proposed method, the parameters of the HC model defined by equation (2.2), would be identified in real time during teleoperation from contact with a given environment. Once the parameters converge, they are used to update the environment side model in the predictive controller. As the parameters update between different materials, the use of a smooth transition function is implemented to avoid jumps in the reflective force that would poorly affect operation or distract the user. A block diagram of the proposed method is shown in Fig. 4.1. Although this approach is not new, previous studies using online parameter estimation for teleoperation have not fully addressed the problems in its implementation. For instance, although there is large support in the use of the HC model for teleoperation in particular, as reviewed in Section 1.1.4, few have demonstrated a way to estimate the parameters while maintaining the nonlinearities of the HC model [15, 16]. Due to the challenge of nonlinear parameter identification, an alternate approach is to linearize the HC model to make it suitable for estimation with least squares techniques such as in [27, 28, 29, 30, 31, 65]. However, linearization assumptions can limit the application of these methods, and naturally have increased error as they do not truly capture the nonlinearities.

Depending on the application, either nonlinear or linear approaches for parameter estimation may have sufficient accuracy to use when their given assumptions are met. Nonetheless, it is important to make the distinction that estimation does not provide control stability. Moreover, inaccuracies in estimation reduce stability margins, and methods requiring long convergence times or sufficient excitation may further disrupt performance when used in a teleoperation system. Thus, a method that provides both stability as well as parameter

convergence with minimal excitation requirements is of great interest.

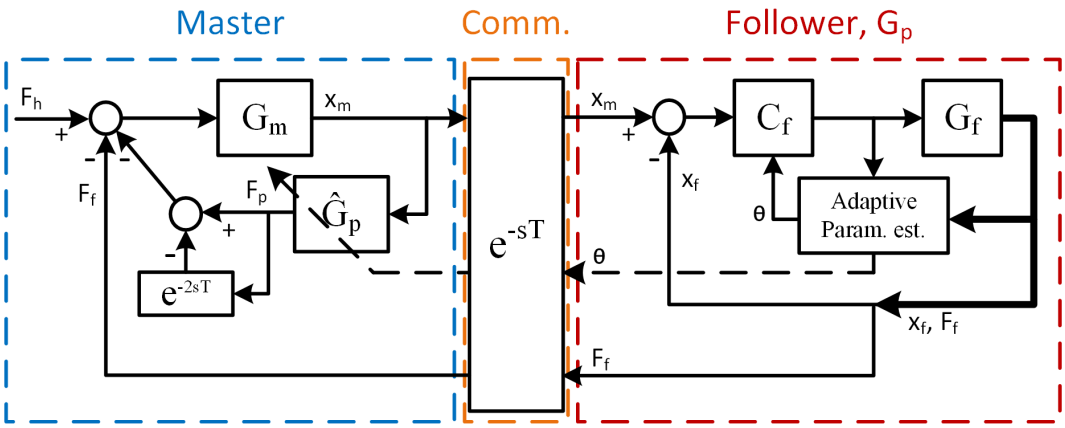

Figure 4.1: Block diagram of environment estimation control architecture.

The work in this chapter first examines and compares the use of various nonlinear parameter estimation methods to identify the parameters of the HC model. Next, a new linearization method that overcomes previous limitations is proposed. Both the nonlinear and linear methods are discussed and compared for use in a teleoperation system. Finally, a new adaptive control and parameter identification approach that does not require persistent excitation is examined.

4.1 Nonlinear Estimation Methods

The nonlinear estimation methods examined involved output error optimization and Kalman filtering. Specifically the methods studied were gradient descent, Levenberg-Marquardt, EKF, and UKF. The algorithms for these methods are detailed in Section 2.5 for reference. For the output error optimization, the quadratic cost function being minimized was

$$r = (h - F)^2,$$

where h is the measured or simulated force, and $F = K\delta^n + B\delta^n\dot{\delta}$ is the modeled force. At each time step an update to the parameter vector $\theta = [K, B, n]^{\mathrm{T}}$ is calculate.

For the Kalman methods, simultaneous state and parameter estimation was implemented by augmenting the state matrix as

$$x = [\delta, \dot{\delta}, K, B, n]^{\mathrm{T}}.$$

Putting this in a discrete form for the next update gives

$$x_k = f(x) = \begin{bmatrix} \delta_{k-1} + \dot{\delta}_{k-1}\Delta t \\ \dot{\delta}_{k-1} \\ K_{k-1} \\ B_{k-1} \\ n_{k-1} \end{bmatrix} + q_k,$$

with the observation equation

$$h_k = \begin{bmatrix} F_k \\ \delta_k \end{bmatrix} + r_k \quad = \begin{bmatrix} K_{k-1}\delta_{k-1}^{n_{k-1}} + B_{k-1}\delta_{k-1}^{n_{k-1}}\dot{\delta}_{k-1} \\ \delta_{k-1} + \dot{\delta}_{k-1}\Delta t \end{bmatrix} + r_k.$$

4.2 Chebyshev Polynomial Approximation

To overcome the shortcomings of the Haddadi linearization method an approximation using Chebyshev polynomials is proposed. By using Chebyshev polynomials to approximate δ^n, better performance is achieved in comparison to the Quad Poly linearization in [31] as well.

The Chebyshev series is a set of polynomials that form an orthonormal functional basis. They are particularly well suited for approximating other functions with periodicity. The Chebyshev polynomials of the first kind are defined by

$$T_n(x) = \cos[n\cos^{-1}(x)], \quad x \in [-1, 1], \quad n = 0, 1, 2 \ldots.$$

This leads to the property

$$T_n(\cos\theta) = \cos(n\theta), \quad \theta \in [0, \pi], \quad n = 0, 1, 2 \ldots.$$

The first five Chebyshev polynomials are

$$\begin{aligned} T_0(x) &= 1, \\ T_1(x) &= x, \\ T_2(x) &= 2x^2 - 1, \\ T_3(x) &= 4x^3 - 3x, \\ T_4(x) &= 8x^4 - 8x^2 + 1. \end{aligned}$$

Chebyshev polynomials of the first kind are orthogonal with respect to $1/\sqrt{1-x^2}$, giving

$$\int_1^1 \frac{T_n(x)T_m(x)}{\sqrt{1-x^2}}dx = \begin{cases} \pi, & n=m=0 \\ \frac{\pi}{2}, & n=m\neq 0 \\ 0, & n\neq m. \end{cases}$$

The exponential term in the HC model is approximated using Chebyshev polynomials leading to

$$F_{\text{env}} = K\delta^n + B\delta^n\dot{\delta} \simeq \sum \alpha_i T_i(\bar{x}) + \sum \beta_i T_i(\bar{x})\dot{\delta}, \tag{4.1}$$

where $\bar{x}$ is a normalization ensuring the psudo penetration is on the interval [-1,1], and $i = 0, 1, 2, \ldots, n$. The coefficients α_i and β_i are computed by the projections

$$\alpha_i = N_\delta N_\pi K \int_0^{L_\delta} \frac{\delta(\bar{x})^n T_i(\bar{x})}{\sqrt{1-\bar{x}^2}}d\bar{x},$$
$$\beta_i = N_\delta N_\pi B \int_0^{L_\delta} \frac{\delta(\bar{x})^n T_i(\bar{x})}{\sqrt{1-\bar{x}^2}}d\bar{x},$$

where L_δ is an arbitrarily defined penetration limit for a given application, $N_\delta = 2/L_\delta$ is a scaling for the normalization of the penetration, $\bar{x} = \delta N_\delta - 1$, $(\delta(\bar{x}) = \frac{\bar{x}+1}{N_\delta})$, and N_π is a scaling for the orthogonality property with $N_\pi = 1/\pi$ when $i = 0$ and $N_\pi = 2/\pi$ otherwise.

The Chebyshev approximation can easily be put into a form that is convenient for parameter identification

$$F_{env} = \theta^{\mathrm{T}}\varphi,$$

with $\theta = [\alpha_i, \ldots, \alpha_n, \beta_i, \ldots, \beta_n]^{\mathrm{T}}$ and $\varphi = [T_i(\bar{x}), \ldots, T_n(\bar{x}), T_i(\bar{x})\dot{\delta}, \ldots, T_n(\bar{x})\dot{\delta}]^{\mathrm{T}}$.

Naturally, a better fit is achieved with a greater number of terms as depicted in Fig. 4.2. However, this in turn comes at the cost of requiring a greater excitation for convergence. To alleviate the need of persistent excitation with increased terms, a method developed by [35] is applied and presented in Section 2.8.

4.3 Comparison of Estimation Methods

To evaluate the performance of both linear and nonlinear HC estimation methods a simulation study is carried out for a simplified second order remote system in contact with a stationary environment in MATLAB and Simulink. The trajectory used for the contact was $x_{\text{d}} = 0.1 + 0.05\sin(2t)$. Soft material parameter values of $K = 300$, $B = 122$, and $n = 1.5$ were arbitrarily chosen for the simulation. Table 4.1 gives the results of the simulation providing the estimation error of the contact force and whether convergence was achieved.

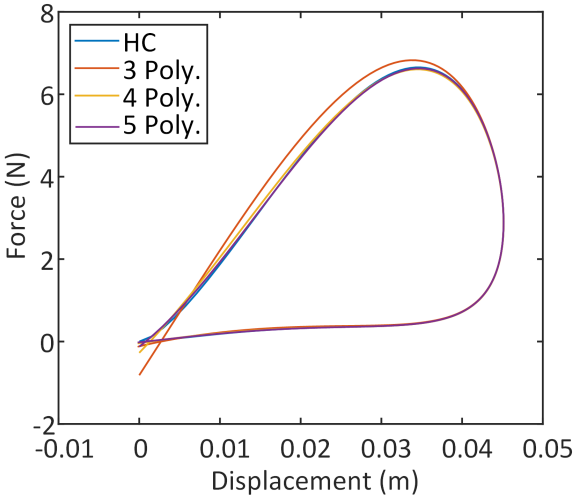

Figure 4.2: Comparison of Chebyshev polynomial approximation of the HC contact model using the first 3, 4, and 5 polynomials of the first kind, K = 300, B = 122, n = 1.5.

The parameter mean and variance of the last 100 updates is also provided for methods that recover K, B, and n.

Table 4.1: Simulation results of linearized and nonlinear HC parameter estimation methods.

Method	Convergence		Force MSE
Haddadi	$K_\mu = 299.231$ $B_\mu = 121.285$ $n_\mu = 1.499$,	$s_K^2 = 1.633$ $s_B^2 = 4.207$ $s_n^2 = 1.350\text{E-}6$	1.219E-5
Quad Poly	yes		8.064E-3
Chebyshev RLS	yes		1.922E-3
Chebyshev KF	yes		5.820E-5
Gradient Descent	$K_\mu = 312.532$ $B_\mu = 127.644$ $n_\mu = 1.513$,	s_K^2=1.379E-2 s_B^2=2.233E-5 s_n^2 =5.574E-6	1.551E-2
Mini Batch LM	$K_\mu = 299.081$ $B_\mu = 119.974$ $n_\mu = 1.499$	$s_K^2 = 1.207$ $s_B^2 = 2.365$ s_n^2 =1.011E-6	1.104E-5
EKF	no		2.014E-7
UKF	no		1.758E-5

For the nonlinear methods, no convergence was achieved with the EKF and UKF. The influence of the exponential term particularly proved too sensitive for the method to estimate. Various cases were run for different magnitudes and parameter values as well as permutations of having one, two, or all parameters unknown (n known with K & B unknown vs. K known with n & B unknown etc.). The trials resulted in convergence as long as at least

one parameter is known. However, when all three parameters are estimated, the tuning of the covariance matrices proved to be too sensitive to achieve convergence, and at best parameters would oscillation around a steady state value with an amplitude that made them unusable. Although the parameters did not converge, in all cases the environmental force of the HC model was estimated with high accuracy. Perhaps this is why the results of [33] that implement a UKF only show the estimated force, and the work in [76] assumes a value for n in their EKF.

On the other hand, both the gradient descent and LM optimization were able to recover the parameters with varying degrees of error. However, a few modifications to the algorithms had to be made to achieve sufficient results. Optimization algorithms depend greatly on the learning rate used during the update. For stable steps towards a minimum the maximum learning rate must be limited to

$$\alpha < \frac{2}{\lambda_{\max}},$$

where $\lambda_{\max}$ is the largest eigenvalue of the cost function's Hessian matrix $H = \nabla^2 r(\theta)$. Using a constant learning rate did not achieve good performance and resulted in small parameter updates that would require very long estimation times. Thus, a varying learning rate was used that updated at each iteration to optimize the learning rate α along a line $F(\theta_k + \alpha_k p_k)$, where p_k is the search direction [77]. This results in the learning rate being calculated at each step as

$$\alpha_k = \left.\frac{J^{\mathrm{T}} J}{J^{\mathrm{T}} H J}\right|_{\theta_k}.$$

This improved the update step, but due to the different magnitudes of the parameters, a scaling factor had to be applied to the update. Finally, since the gradient descent method is implemented online with one new data point per time step, it is susceptible to converging at a local result. To overcome this, the initial conditions for the gradient descent method were chosen on the same relative magnitude as the true parameters, $\theta_0 = [100\ 100\ 1]$. The number of iterations for the gradient descent was kept constant at 1000 iterations per time step. Out of the nonlinear estimation methods investigated, the LM algorithm proved to have the fastest convergence and greatest accuracy in force estimation. The LM algorithm is implemented using the built in LSQNONLIN MATLAB function. However, having one data point per time step results in low robustness to noise. To overcome this, a mini-batch approach is used. This is implemented with a tapped delay line of 500 samples for each iteration of the LM algorithm. The number of iterations and function calls for each time step is controlled by the LSQNONLIN function. The parameter convergence and estimation error for both the gradient descent and the mini batch LM is dipicted in Fig. 4.3. For the linearized HC methods, the proposed Chebyshev polynomial approximation, utilizing both RLS and KF for the estimation, was compared to the Haddadi and Quad Poly linearization. Since the Chebyshev approximation uses a set of polynomials for both $K\delta^n$ and $B\delta^n$, there are more parameters to identify than in the Haddadi and Quad Poly methods. However, since the Chebyshev Polynomial approximation has a convenient algebraic form, it is suitable

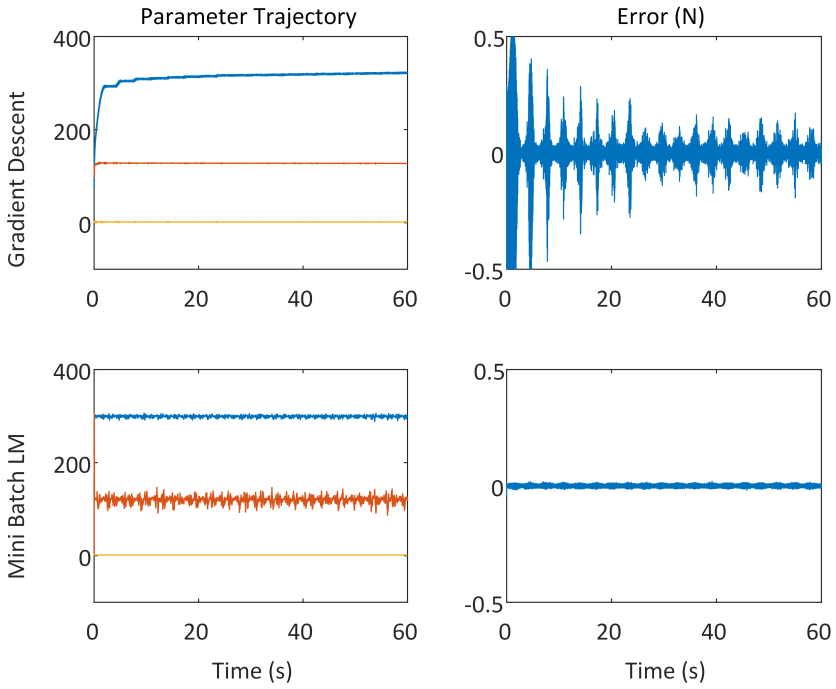

Figure 4.3: Comparison of estimation techniques for Nonlinear HC parameter identification. K = 300, B = 122, n = 1.5.

for estimation with a Kalman filter as well as RLS. This results in faster convergence and less error using the former in comparison to the Quad Poly method. When compared to the Haddadi method, although the proposed approach has slightly longer convergence times, it has the benefit of not being limited by a minimum penetration depth and loading rate with a comparable error in force estimation. This allows for a greater range of application in practical use. The parameter trajectories as well as the resulting error for these methods is shown in Fig. 4.4.

Ultimately, the mini-batch LM method has the fastest convergence times and lowest error out of all the estimators used. Since it maintains the nonlinear form of the HC parameters as well, it is the best candidate from a performance standpoint. On the other hand, in terms of implementation it can be the most computationally costly as the simulation had a maximum number of iteration and function calls at 134 and 603 respectively. In comparison, the proposed Chebyshev approximation can be a simplified alternative with Kalman filtering that has similar accuracy and reasonable parameter convergence times, with no limiting assumptions for the linearization. Thus, depending on bandwidth and convergence criteria, either of the proposed Chebyshev approximation or LM method are improved alternative estimation methods for the HC model that can be used in the teleoperation system.

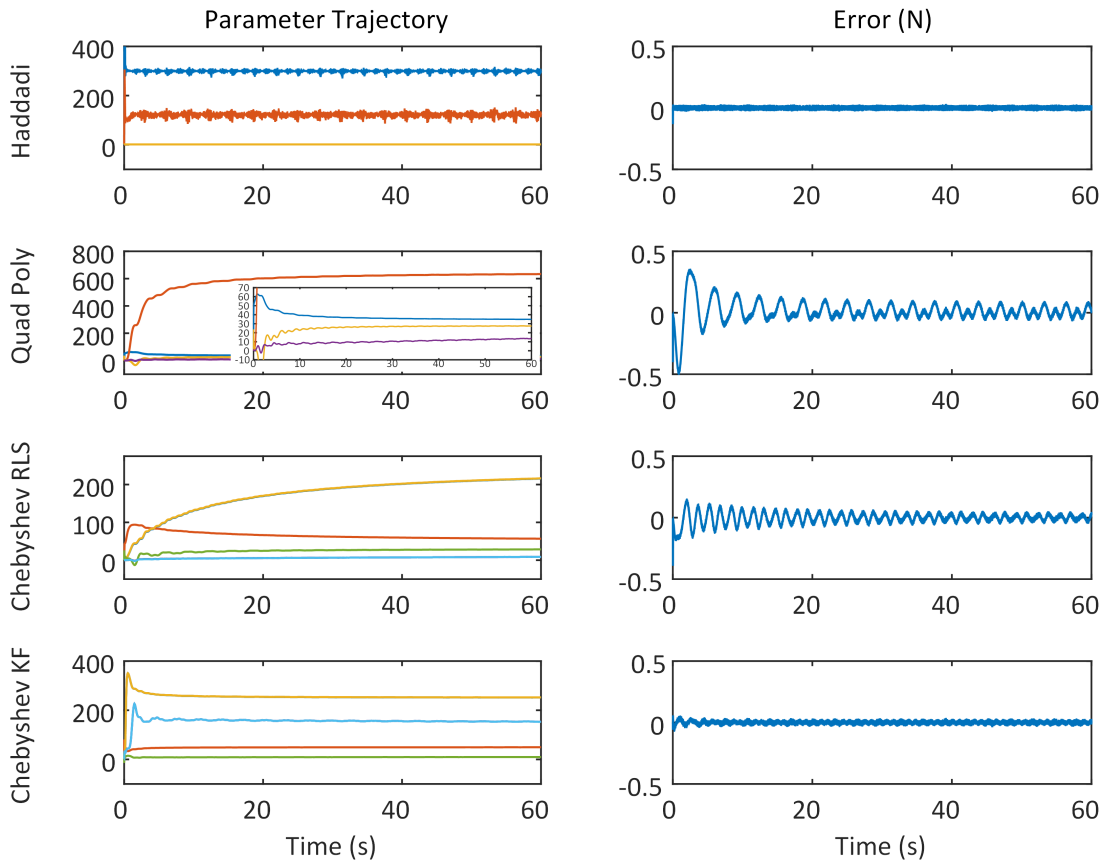

Figure 4.4: Comparison of estimation techniques for linearized HC parameter identification. K = 300, B = 122, n = 1.5.

4.4 Contact Force Parameter Estimation and Remote System Control

Although the estimation methods above provide good parameter convergence and accuracy, they have the drawback of requiring sufficient excitation for parameter convergence. Moreover, they do not address the control of the remote side system. To address these shortcomings of the above estimation techniques, the use of adaptive parameter estimation with nonlinear swapping and data accumulation is proposed as a solution. This method was originally introduced in [35] for state parameter estimation and is detailed Section 2.8. The proposed method as applied here will be refer to as the guaranteed adaptive parameter estimation (GuAPE) method. The GuAPE method modifies the original implementation to estimate the contact force model parameters, influenced by the control, instead of state parameters as originally formulated. The following presents the derivation for applying the

adaptive parameter estimation method to a general second order system with an externally applied force.

Given a system of the form

$$\begin{aligned}\dot{x}_1 &= x_2,\\ \dot{x}_2 &= -a_1 x_1 - a_2 x_2 + b(u - F_\mathrm{e}),\end{aligned}$$

with states x_1 and x_2 as the position and velocity, the external force F_e is modeled as the Chebyshev polynomial approximation of the nonlinear HC environment force as defined in eqn. (4.1). Nonlinear backstepping is applied to develop a controller for the system to track a reference trajectory with the error defined as

$$z_1 = x_1 - y_r,$$

where $y_r = x_{r1}$ from a second order reference system

$$\dot{x}_r = A_r x_r + Br,$$

with $x_r = [x_{r1}\ x_{r2}]^\mathrm{T}$ and A_r Hurwitz. x_2 is used as a virtual control with the stabilizing function chosen as

$$\alpha_1 = -c_1 z_1 + \dot{y}_r.$$

Defining $z_2 = x_2 - \alpha_1$, the error dynamics become

$$\begin{aligned}\dot{z}_1 &= \dot{x}_1 - \dot{y}_r = x_2 - y_r = z_2 - c_1 z_1,\\ \dot{z}_2 &= \dot{x}_2 - \dot{\alpha}_1 = -a_1 x_1 - a_2 x_2 + bu - b\theta^\mathrm{T}\varphi - \dot{\alpha}_1,\end{aligned}$$

where $\dot{\alpha}_1 = -c_1 z_1 + \ddot{y}_r = -c_1 x_2 + c_1 \dot{y}_r + \ddot{y}_r$ making

$$\dot{z}_2 = -a_1 x_1 - a_2 x_2 + bu - b\theta^\mathrm{T}\varphi + c_1 x_2 - c_1 \dot{y}_r - \ddot{y}_r.$$

Choosing the Lyapunov function as

$$V_1(z_1, z_2) = \frac{1}{2} z_1^2 + \frac{1}{2} z_2^2,$$

$$\dot{V}_1 = z_1 \dot{z}_1 + z_2 \dot{z}_2 = z_1 z_2 - c_1 z_1^2 + z_2(-a_1 x_1 - a_2 x_2 + bu - b\theta^\top \varphi + c_1 x_2 - c_1 \dot{y}_r - \ddot{y}_r).$$

To ensure that $\dot{V}$ is negative definite the control input is selected as

$$u = \frac{1}{b}(-z_1 - c_2 z_2 + a_1 x_1 + a_2 x_2 + b\theta^\mathrm{T}\varphi - c_1 x_2 + c_1 \dot{y}_r + \ddot{y}_r).$$

Substituting the estimates in the control the error dynamics are now

$$\dot{z}_1 = z_2 - c_1 z_1,$$
$$\dot{z}_2 = -z_1 - c_2 z_2 - b\tilde{\theta}^{\mathrm{T}}\varphi,$$

with $\tilde{\theta} = \theta - \hat{\theta}$. The parameter update is now obtained from the Lypunov function

$$V_2(V1, \tilde{\theta}) = \frac{1}{2}z_1^2 + \frac{1}{2}z_2^2 + \frac{1}{2}\tilde{\theta}^{\mathrm{T}}\Gamma_\theta^{-1}\tilde{\theta},$$
$$\dot{V}_2 = z_1\dot{z}_1 + z_2\dot{z}_2 + \tilde{\theta}^{\mathrm{T}}\Gamma_\theta^{-1}\dot{\tilde{\theta}} = -c_1 z_1^2 - c_2 z_2^2 - \tilde{\theta}^{\mathrm{T}}(z_2 b\varphi + \Gamma_\theta^{-1}\dot{\hat{\theta}}), \tag{4.2}$$

giving the update law

$$\dot{\hat{\theta}} = -\Gamma_\theta z_2 b\varphi. \tag{4.3}$$

From here, the nonlinear swapping and data accumulation filters $\dot{W}_x$, $\dot{\bar{\epsilon}}$, $\dot{Q}$, $\dot{\psi}$, with tuning parameters Λ_x, Λ_r, R_x, K_x, are applied using the same definition as in Section 2.8. The estimator dynamics specifically for this system are now defined as

$$\dot{\hat{x}} = Ax + B(u - \hat{\theta}^{\mathrm{T}}\varphi) - \Lambda_x(X - \hat{X}) + K_x^{-1}W_x\dot{\hat{\theta}}.$$

The parameter update law in equation (4.3) is now modified to give

$$\dot{\hat{\theta}} = \Gamma_\theta(-z_2 b\varphi + \mu),$$

where the modifier μ is now expressed in known quantities as

$$\mu = M\tilde{\theta} = W_x^{\mathrm{T}}\Gamma_x\varsigma_x + Q^{\mathrm{T}}\Gamma_\psi\tilde{\psi}.$$

Now, when Q achieves full rank M is positive definite. This makes the Lyapunov derivative from (4.2) become $\dot{V} = -z^{\mathrm{T}}Cz - \tilde{\theta}^{\mathrm{T}}M\tilde{\theta}$, where C is a positive definite matrix of control gains c_1 & c_2 for $z = [z_1\ z_2]^{\mathrm{T}}$. Since $\dot{V}$ is negative definite, the estimation error converges to zero according to the LaSalle-Yoshizawa theorem [72].

4.5 Master Side Model Update

When the environment parameter estimation is utilized in the Smith predictor based control architecture, there are a few practical considerations that must be addressed. First, an initial a priori estimate of the parameters must be made to close the loop in the teleoperation system. Second, once new parameters converge there can be a jump in the estimated force, and care must be taken that this transition does not disrupt operation. To provide a smooth transition and maintain continuity in the signal, the use of a Sigmoid function depicted in Fig. 4.5 is proposed. The function is defined as

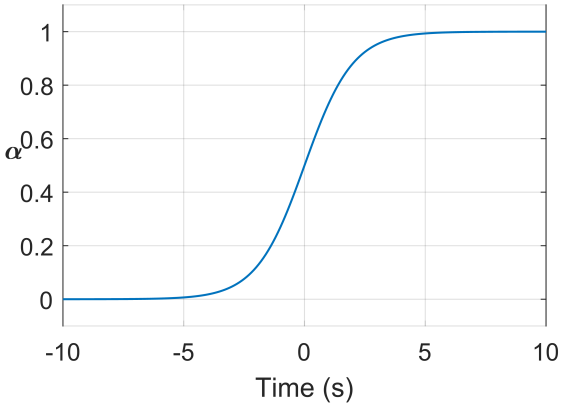

Figure 4.5: Example Sigmoid function from eqn. (4.4) with $\gamma = 1$, $\beta = 0$.

$$\alpha = 1 - \frac{1}{1 + e^{\gamma(t-\beta)}},$$

where γ and β are a scaling factor and offset, respectively, to change the slope and timing of the parameter transition. Once a new parameter set is converged, α is used to transition from the initial parameters to the new parameters as follows

$$\begin{aligned} F_1 &= \theta_1^{\mathrm{T}} \varphi, \\ F_2 &= \theta_2^{\mathrm{T}} \varphi, \\ F &= \alpha F_2 + (1 - \alpha) F_1, \end{aligned}$$

where F is the haptic force being sent to the user. The criteria for when a new parameter set is ready to be used can be heuristically determined based on application. This can be very helpful depending what estimation method is used by allowing an updated force to be sent smoothly, even while parameters are changing to minimize the delay between contact and haptic force rendering. The update criteria used here is when the root mean square error between the estimated and measured force is less then the desired tolerance.

4.6 Teleoperation Simulation

Since the adaptive backstepping approach addresses both control and estimation with guaranteed parameter convergences based on Lyapunov methods, it is chosen as the main method to pursue for a haptic time delayed system. The GuAPE approach was applied to a full haptic teleoperation system with time delay in simulation using Simulink. The master and remote devices were generalized as identical second order mass spring damper systems. The derivation in Section 2.8 was used for the control and update laws. The predictive controller for the teleoperation system was implemented discretely at 1 kHz. The contact

location was assumed to be known a priori at $x_e = 0.01$ m. The user input force was a chosen as $F_u = 2.5 + 0.5\sin(6t)$. The tuning parameters for the simulation were $\Gamma_\theta = 10$, $\Gamma_x = R_x = 30I_{[2\times2]}$, $\Gamma_\psi = 250I_{[6\times6]}$, $Q_r = 20I_{[6\times6]}$, $K_x = 2I_{[2\times2]}$, $\Lambda_r = -10I_{[6\times6]}$, and $\Lambda_x = -20I_{[2\times2]}$.

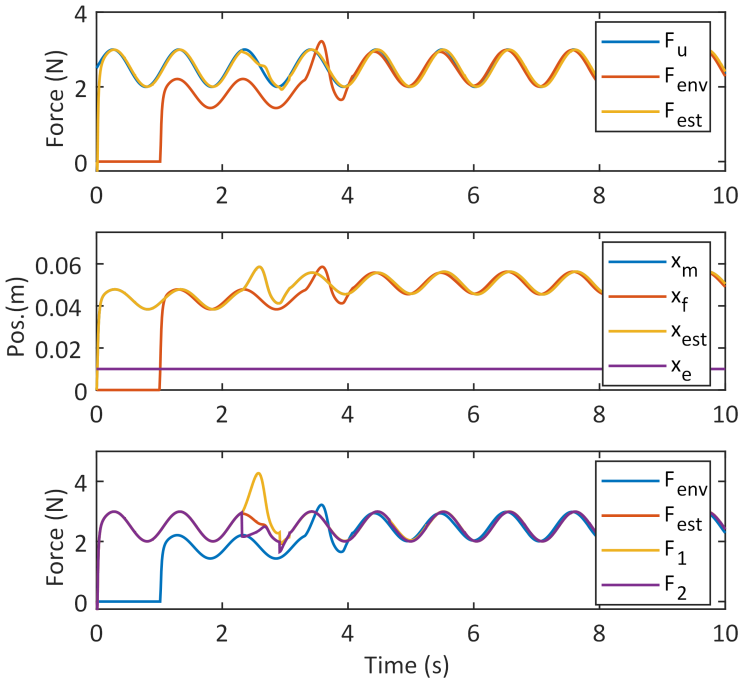

Figure 4.6: Force and position results for 2 s RTT simulation with adaptive parameter estimation.

Figure 4.6 shows the system performance with the proposed control architecture for a round trip time delay of 2 seconds. The adaptive backsteping control law achieved asymptotic position tracking of the master signal with a MSE of 1.739E-5. An initial guess for parameters were chosen greater than the true parameters resulting in an overestimation of the environment contact force. This initial guess was corrected at approximately 2.5 s when the estimated force error was sufficiently small to send the parameter update and the estimated force transition can be seen in the bottom subplot in Fig. 4.6. After the parameters adapt sufficiently, the estimated force converges to the environment force. Using the predictor force with the reflected force in the SP resulted in more oscillations, so only the predicted force is used in the control scheme.

The true HC parameters used were $K = 300$, $B = 122$, $n = 1.5$. Projecting this onto the Chebyshev polynomial approximation using the first 3 polynomials results in the true parameters $\theta = [4.026, 4.831, 0.690, 1.63738, 1.964, 0.280]$ for $N_\delta = 20$.

The parameter adaptation is shown in Fig. 4.7. The final values after ten seconds for the

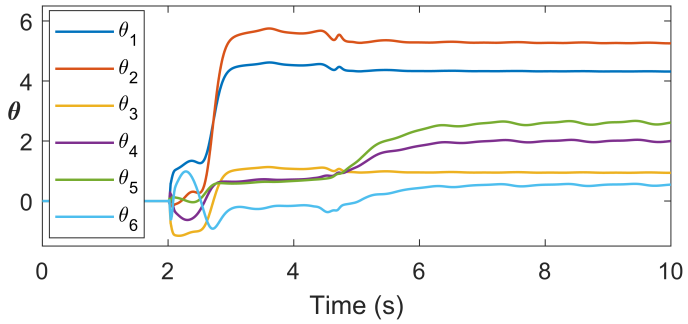

Figure 4.7: Parameter Convergence for 2 s RTT simulation with adaptive parameter estimation.

estimates are $\hat{\theta} = [4.315, 5.255, 0.940, 1.999, 2.614, 0.548]$, with a force estimation MSE of 4.425E-4 N. The difference in the parameter values is in part a result of using only the first three polynomials for the estimation as the lower number of terms must be weighted differently to make up for the higher order nonlinearity matching. M was observed to be positive definite for the entire duration of estimation, thus ensuring parameter convergence. Overall, these results show promise for the GuAPE method to be used for estimation of the Chebyshev approximated HC parameters. Of note is the is the stability and performance of this method in a RTT of 2 s. Moreover, the ability for the Smith predictor to smoothly transition between parameter updates to make up for incorrect initial values gives confidence in the robustness of this architecture for use in application.

4.7 Conclusion

This work provided a comparative analysis on various methods to estimate parameters of the HC model. A review of nonlinear estimation methods that has been missing in literature was provided along with a quantitative analysis from simulation. Results showed that Kalman filter based methods cannot recover the model parameters, but can provide very accurate force estimation. Additionally, a new linearization method that uses Chebyshev polynomial approximation was proposed and compared to existing methods. Simulation results show its capability in good convergence time and accuracy while not being limited to the linearization assumptions of current methods. Moreover, an adaptive parameter estimation technique that provides control through backstepping with guaranteed parameter estimation was proposed and evaluated in a full teleoperation system simulation. Results showed good tracking of the desired master position with parameter convergence resulting in high accuracy force estimation. Finally, a method to switch between parameter updates in the predictive controller was introduced that showed good robustness in simulation.

Chapter 5

Semi-Autonomous Teleoperation

D. Budolak, R. Chauhan, and P. Ben-Tzvi, "Semi-Autonomous Teleoperation, Guidance, and Obstacle Avoidance With Path Adherence," in *Volume 5A: 43rd Mechanisms and Robotics Conference*, pp. 1–7, American Society of Mechanical Engineers, 8 2019 [78].

As time delay in teleoperation systems continues to increase, the performance of the system degrades from modeling error and disturbances. Because of this, semi-autonomous capability on the remote side is necessary to bridge the gap in performance in large delays. Semi-autonomous assistance in teleoperation systems also have the benefit of reducing the load on the user by accomplishing sub tasks autonomously, or by applying guidance and additional feedback. Some of the aforementioned methods discussed in Section 1.1.6 demonstrate great potential as options for decreasing user effort, but they have not been synthesized for a holistic shared control or semi-autonomous framework. This work proposes the use of path planning with user intention recognition for guidance and obstacle avoidance for semi-autonomous teleoperation. The novelty of this work is twofold. First, a projection based predictor for user intention recognition is implemented for target identification based on user motion. Second, a control architecture for gross motion automation with subtask execution is developed for assistive teleoperation based on an optimal trajectory from an assumed path planner. The target identification runs continuously allowing for target correction, with the user controlling shifting between direct teleoperation or assisted control. By focusing on the gross motion, there is no need to realign pose frames as in situations with auto grasping. Moreover, this takes greater advantage of the teleoperation paradigm by leveraging user knowledge to execute complex tasks in unstructured environments, while reducing the burden on the user with trivial motion execution. Sub tasks of bounding the workspace and singularity avoidance are applied to the user as haptic feedback. A user study for a pick and place operations is conducted to evaluate the proposed method's performance and user perception of the framework.

5.1 High Level System Architecture

In this semi-auto control architecture, a state machine is used to direct haptic control switching. During the selection state, user motion is used to predict which pre-identified target

the user is trying to move to. Once identified, the follower automatically moves there using an assumed trajectory from a path planner that avoids obstacles in the path. Once the target is reached the state transitions to direct control with haptic guidance to bound the workspace and avoid singularities. During the gross motion automation state, the user can continuously correct the target selection. The work presented here focuses on applying the proposed semi-autonomous teleoperation scheme to a real workspace synchronization of a heterogeneous master follower system, with a non-redundant follower. The formulation given below is developed for the experiment, but is presented generally and can be scaled to other systems.

Figure 5.1 depicts the proposed architecture summarized above, where FK and IK refer to the forward and inverse kinematics respectively. User input to the master haptic device is sent to the follower where a supervisor governs whether to navigate to a target autonomously based on the user input (State 1), or whether the target location has been reached and the user is given direct control of the follower with haptic feedback (State 2). The user is able to switch between states at any given time with a button on the master device; this could alternatively be placed on the master side computer. In this architecture, the master position is sent to the remote (referred interchangeably as the follower), where a PID controller is used to control each joint of the manipulator. The follower side controller is formulated for a heterogeneous master-follower system where the master workspace is much smaller than the follower workspace. Thus, only a delta position is sent, such that the user can choose when the master and follower are linked in order to re-orient themselves and continue operation when they have reached the end of the master's workspace. To not interfere with the operator, virtually imposed haptic forces are reflected back on to the user only for the workspace bounding sub task.

5.1.1 User Intention Recognition

To identify the target that the user is trying to move towards, the heuristic in eqn. (5.1) is used. It is the maximization of the dot product between the master velocity and the vector from the slave end effector to each of the targets. It takes the form of

$$i = \arg\max_{i}(\vec{v} \cdot \vec{r}_{x,i}) \tag{5.1}$$

where i is the determined target, $\vec{v}$ is the velocity of the master, and $\vec{r}_{x,i}$ is the vector pointing from the slave end effector to the i^{th} target. To make the system agnostic to the magnitude of $\vec{v}$ and $\vec{r}_{x,i}$, each of them is normalized prior to the evaluation of the dot product. Assuming small sensor noise and a perfectly direct user heading, the above identifier would only fail to distinguish user intent in the case of exact symmetry such that the value of $\vec{v} \cdot \vec{r}_{x,i}$ is not unique. This extends to the case that the end effector and multiple targets are exactly in line with each other. Neither of these cases is highly likely and as such, the proposed identifier can be used to adequately determine user intent.

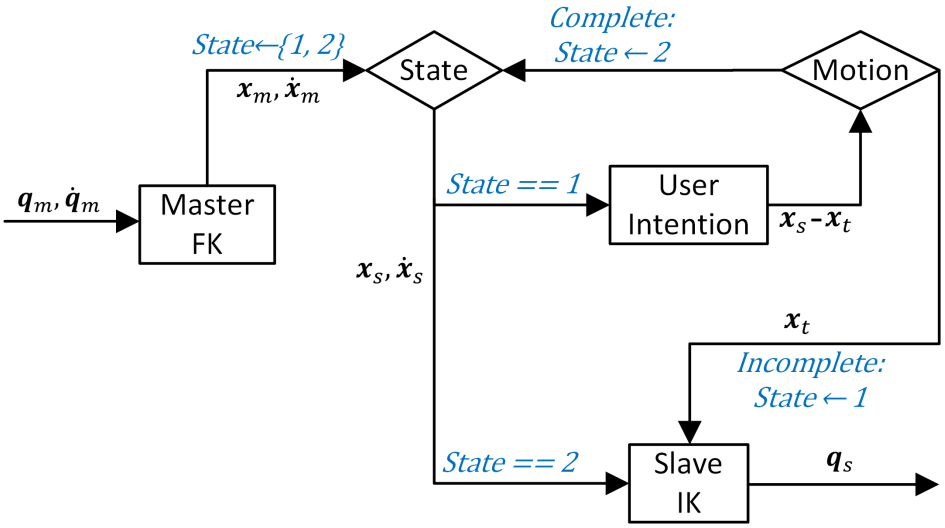

Figure 5.1: Semi-autonomous assistive architecture diagram with supervisory state based control for recognizing user intention and motion execution. Subscripts m, s, and t refer to the master, slave, and target respectively.

5.1.2 Haptic Guidance Rendering

To ensure that the user does not crash the end effector into the ground, the virtual force is defined to be

$$F_{\mathrm{H}} = \begin{cases} Ke + B\dot{e}, & \text{if } z_{\mathrm{l}} > x_{\mathrm{s}} > 0 \\ 0, & \text{if } z_{\mathrm{l}} < x_{\mathrm{s}}, \end{cases} \tag{5.2}$$

where $e = z_{\mathrm{l}} - x_{\mathrm{s}}$ for the slave side position vector x_{s}, and z_{l} is the set lower workspace limit in the $\hat{k}$ direction.

For workspace boundary singularities, the follower evaluates whether $|x_{\mathrm{m}}| \leq L$, where x_{m} is a vector of the end effector pose, adjusted to be with respect to the manipulator's shoulder joint, and L is the workspace limit from joint q_2 such that

$$\sqrt{x^2 + y^2 + (z - L_1)^2} \leq L_2 + L_3 + L_4.$$

R is set to be the boundary radius for the virtually imposed haptic force. If $R < |x_{\mathrm{m}}| < L$, the haptic force guides the user back towards inside the workspace, with the force asymptotically reaching infinity at the workspace boundary as

$$F = F_{\mathrm{H}} \frac{-\vec{r}\,\gamma}{(|\vec{r}| - R)^n} \quad , \quad n = \text{even} \tag{5.3}$$

where γ is a tuning parameter to scale how quickly the force approaches the asymptote. This ensures that the user does not reach the workspace singularity. All of the haptic forces are limited to the output of the master haptic device, ensuring safe operation.

5.1.3 Follower Side Control

Although in non-delayed systems position-velocity and velocity-velocity control architectures are often used, they are known to lose transparency when time delay is present. For scaling to time delayed applications, the proposed control architecture mirrors a force position scheme where the follower tracks the master position command with haptic forces reflect onto the user from the haptic device. In the proposed method, the follower workspace is much larger than the master's, thus, a method must be employed to allow the user to reset the master position after running out of motion due to kinematic constraints. To accommodate this, a button is used to synchronize the master and follower, linking the end effectors and zeroing the current master position, such that only subsequent relative positions $x_{\mathrm{m}} = \Delta x_{\mathrm{h}}$ are sent.

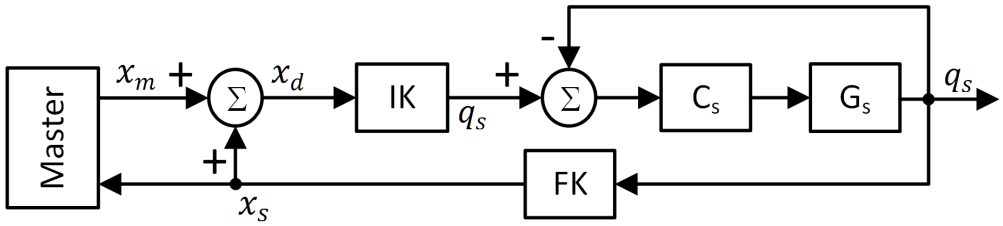

Figure 5.2: Slave side position controller for the workspace pose command. C_{s} and G_{s} are the slave low level controller and plant. IK and FK refer to the inverse and forward kinematics calculation respectively.

On the follower side the assistive control architecture assumes a trajectory from a path planning algorithm. The trajectory is discretized into incremental desired pose commands sent to the follower. The desired slave manipulator pose, whether for direct teleoperation or autonomous trajectory following, is achieved by the position controller depicted in Fig. 5.2. The desired pose x_d is calculated from the current follower position and the delta sent from the master such that $x_{\mathrm{d}} = x_{\mathrm{m}} + x_{\mathrm{s}}$. Joint control is implemented on the follower with a PID controller from the inverse kinematics of the pose. Because the follower robot is not kinematically redundant with the task space equal to the joint space $m = n, \in \mathbb{R}^3$ as the wrist is commanded independent of the end effector position, the inverse kinematics can be solved analytically from geometry instead of using a Jacobian pseudo-inverse. The actual robot position is then calculated based on the forward kinematics model to provide the correct desired pose for the master position command.

5.2 Validation with User Study

To validate the proposed semi-autonomous control strategy, an experiment was conducted for a teleoperation task. Users completed a pick and place task with both the direct control

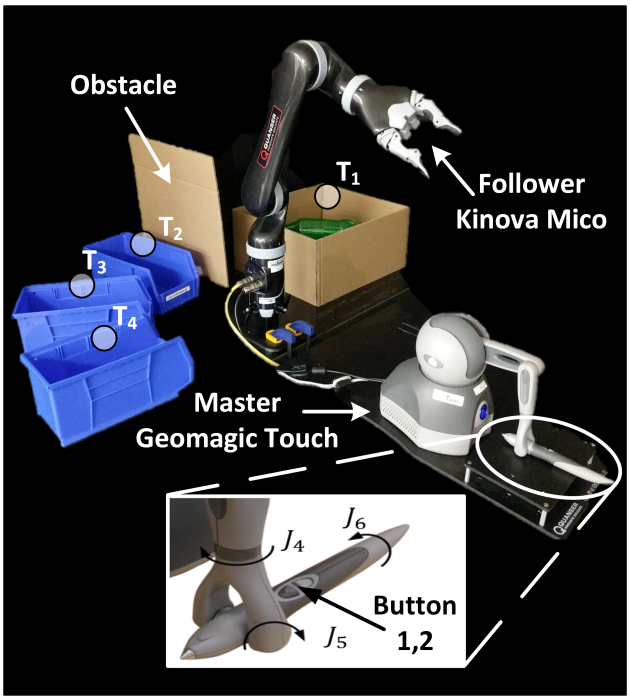

Figure 5.3: Experimental setup with indicated master and follower systems, environmental obstacles, and operational targets (T1-T4).

of the system and the proposed assistive control scheme. Task completion time as well as user perceived effectiveness of the assisted control was evaluated. To compare with previous studies and provide a deeper analysis, the trajectory length and total angular displacement was also evaluated.

5.2.1 Experimental Setup

The experiment used a teleoperation system consisting of a Geomagic Touch [79] as the master haptic device, and a Kinova Mico arm [80] as the follower. The Mico arm is a four DOF manipulator with a two finger gripper attachment. The Geomagic Touch has six DOF but only the first three joints are active. The passive wrist has a stylus held by the user with two buttons for three button modes: top (1), bottom (2), and both buttons held simultaneously (3). The master and follower are implemented on separate computers using MATLAB/Simulink running at 500 Hz. Communication between the master and follower is performed across the network using a UDP protocol to increase communication speed. Although the communication delay is nonzero, it was negligible such that the system is assumed to be without time delay.

A pick and place teleoperation task was conducted that involved grasping an empty water bottle and placing it into one of three containers, while avoiding an obstacle as depicted in

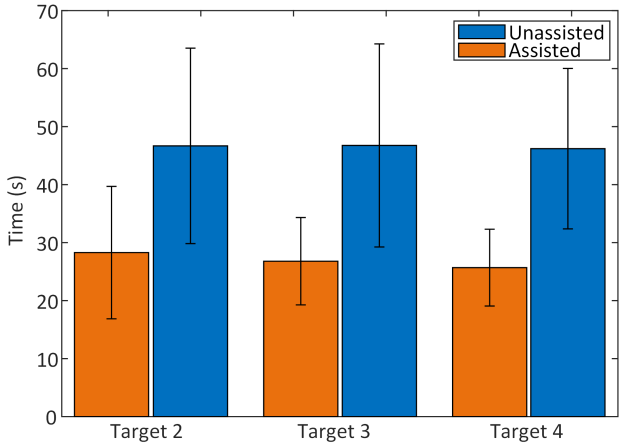

Figure 5.4: Task completion times for assisted and direct control teleoperation. The values of the bars are the mean values and the error bars indicate a single standard deviation.

Fig. 5.3. The bottle was placed in a staging area on a metal block elevating it from the table. For both the direct and assisted trials, the follower started in a home position just above the obstacle in between the containers and the bottle. The user study was carried out with six participants with three trials for each container target for both operation modes, for a total of 18 trials per user. Half of the users had previous experience controlling a teleoperated system.

In the direct control mode, the Geomagic buttons were used to give the user control over more than just the end effector position. While holding Button 3, the end effectors are linked in the Cartesian space. While Button 1 is pressed, motion in the x-axis of the master opens and closes the follower gripper fingers. When Button 2 is held, motion along the y-axis turns the wrist. The previous pose of the follower is held while no buttons are engaged, allowing the user to reorient the stylus to make up for the disproportionate workspaces.

In the assisted mode, the user operated in different machine states. In State 1, the user inputs a motion for the intended target identification. Once a target is identified, the follower autonomously navigates to the target based on an assumed trajectory from a path planner. While the follower is executing the trajectory in State 1, the user can still give direction inputs to select another target. Once the follower has reached a target, the operator regains direct control of operation until switching back into the intention recognition state from any button double click. By employing this method, the user can select when they want the autonomous assistance. In the assisted mode, haptic forces are also generated in the direct control state for sub tasks of avoiding ground collision and staying within workspace boundaries, as defined by equations (5.2) and (5.3).

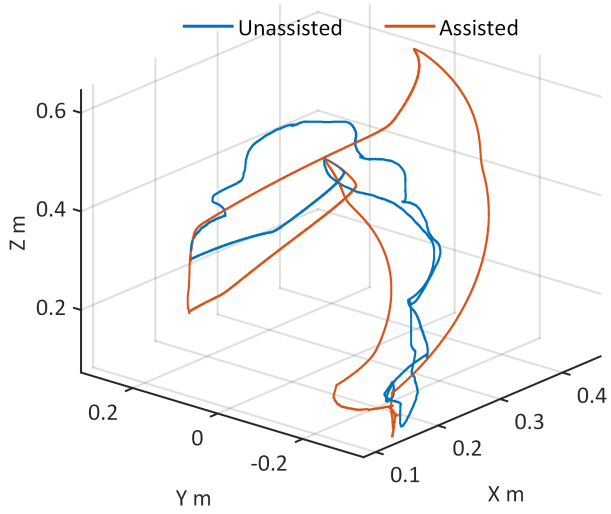

Figure 5.5: Trajectories for direct control and assisted teleoperation of a sample trial to Target 4.

5.2.2 Results and Discussion

The experiment is evaluated by examining the completion time, trajectory length, total angular displacement, and the user's perceived effectiveness of the assisted control mode compared to the unassisted mode. The accuracy of the intention recognition method for predicting the target is also examined. Figure 5.4 shows the mean task completion times for each target for all the users, along with the standard deviation. The completion time was significantly shorter for the assisted mode, with no significant variation between targets. Overall, the assisted control scheme provided great benefit by automating the tedious task of gross manipulation. Traversing the obstacle was substantially accelerated by the assistive control. This method is particularly beneficial in the position based master-follower control scheme, since the user has to readjust when they reach the end of the master's workspace. Because of this, operator skill affected the spread of the data which can be seen in the variance of the completion times, particularly for the unassisted case.

In addition to operator skill, task learning throughout the trials also had an affect on the data. It was observed that users became more proficient in operating the system as trials progressed, resulting in an average completion time reduction of 23.8% for the unassisted case and 35.6% for the assisted case, evaluated from the longest trial in each case for each user. The time reduction was also greater for novice users, with similar improvements between the unassisted and assisted cases of 12.6% and 13.6% reduction in completion times respectively.

The benefit of the proposed method is also evaluated using metrics of the user's motion. Based on the trajectory data in Table 5.1, the proposed method increases the efficiency in task execution by reducing total motion of the task. For all cases, the trajectory length

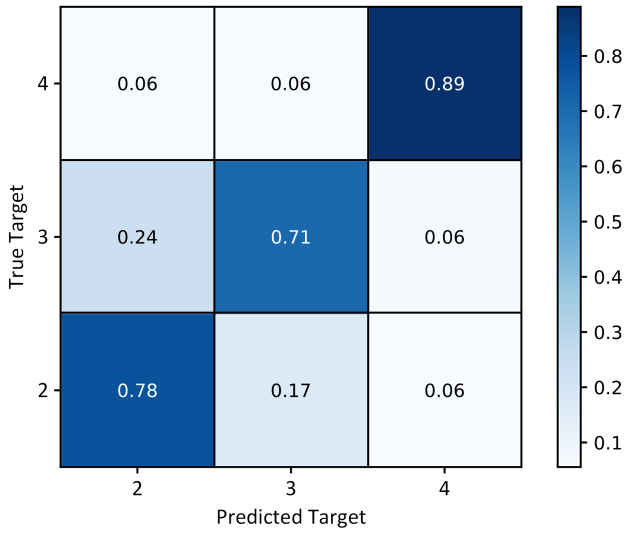

Figure 5.6: Confusion matrix of intended user target prediction.

Table 5.1: Trajectory length and angular displacement comparison.

	Unassisted Length		**Assisted Length**	
	(m)	**(rad)**	**(m)**	**(rad)**
Target 2	2.838	17.622	2.706	14.258
Target 3	3.014	18.793	3.006	15.616
Target 4	3.402	20.781	3.261	16.323
Mean	3.085	19.066	2.991	15.399

was shorter for the assisted mode than the unassisted one. It should be noted however, that the distance to the target and amount of maneuvering about an obstacle affects the overall trajectory length. This can be seen by comparing the trajectory lengths between the different targets where Target 3 as well as the mean vary minimally. On the other hand, the total angular displacement of the joints had a more significant benefit in minimizing motion, which can lead to longer usability of the system by minimizing wear. Naturally, the method of generating the trajectory affects these metrics from the use of optimization and any imposed conditions for safe maneuvering. For instance, the defined trajectories for the experiment ensured that the end effector could clear over the obstacle while maintaining the longitudinal orientation of the grasped bottle, resulting in a larger motion in the z-axis than most users, as depicted in Fig. 5.5.

The feasibility of this method is also supported by the effectiveness of the user intention recognition for target identification. A confusion matrix in Fig. 5.6 shows the accuracy of the method for each target. As expected, the outer targets had the greatest accuracy, as the path to the target has tighter margins to align to a target in between a group of other targets. Thus, the grouping of targets and their distribution can have an impact on the accuracy of the method because of how well users can align their motion. To better distinguish between

tightly packed targets, a score can be used to accumulate confidence in the target with the method, however, this requires more movement along the path before a target is identified, which is a drawback seen in other user intention methods covered in the literature review above. Moreover, the proposed approach allows for selection correction, which was effectively implemented by the users in the study resulting in faster task completion times even if the initial target prediction was incorrect. This also allows for more immersive teleoperation as compared with a supervisory level target selection from the computer.

User perceived effectiveness of the assisted control scheme was also evaluated quantitatively with a standard 5 point Likert scale, as well as qualitatively from the users' comments. An average score of 4.67 was obtained from the users regarding whether they thought the assisted control scheme was more effective in task execution over direct control. All users reported perceiving the assisted control mode as beneficial for the task execution and non obstructive to operation. Additionally, the majority of users reported that the target selection was effective to speed up task execution, even in the few cases where the wrong target was initially selected. However, users did identify the button command on the stylus as difficult to operate at times.

5.3 Conclusion

This work presents a novel approach for assistive teleoperation with a control strategy that automates gross motion tasks with subtask execution, and incorporates an efficient user intention prediction method for target identification. A user study demonstrates the effectiveness of the proposed method as completion times for a pick and place task were significantly improved. Additionally, the user intention prediction proved to be accurate in target identification and a robust solution as it allows for online correction. User perception of the proposed method was positive, and all participants in the study identified the assistive mode to be effective in easing task execution.

Chapter 6

Conclusion & Future Work

The work presented herein examines solutions to prevailing challenges concerning performance, control, and user interaction of time delayed haptic teleoperation systems. Focus was placed on the application of these solutions to a F-P predictive control architecture, which is the most commonly used control scheme in teleoperation. The goal of extending the capabilities and usefulness of such systems was addressed by investigated methods that: 1) enhance performance through the use of an SEA on the remote system, 2) estimate nonlinear and linearized HC model parameters and alternatively provide both control and adaptive parameter estimation, with a robust method for parameter updates to the predictive controller, and 3) reduce user load with semi-autonomous assistive control and user intention prediction.

By augmenting the system with an SEA as the end effector on the remote side, transparency of the system was increased in delays of up to 2 s with stiff environments. The coupling of force and position through the SEA, along with its sensing capabilities also provided promising capabilities with soft and moving environments. Future improvements with this solution can be particularly useful in telesurgery applications for interacting with soft and hard tissue. This work can also be expanded by extending the SEA to a multi-degree of freedom manipulator. Evaluating specific task performance and completion times will be a useful metric to further evaluate the system's practical application. This would also help gather qualitative user data on how compliance affects teleoperation systems.

The proposed SEA system assumes no knowledge of the environment dynamics. To provide better performance with soft environments, estimation of the follower-environment contact force was added to the control architecture to improve the remote side prediction. Various nonlinear estimation methods for identifying the HC model parameters were investigated. Mini-batch optimization techniques, primarily the LM algorithm showed the best performance. However, the list of estimators evaluated in the study was not exhaustive, and many variations of the gradient descent method may provide better performance, such as AMSGrad, Google Adam optimizer, or any of the various optimizers that are commonly used to train neural networks. As an alternate approach, an improved linearization of the HC model that uses Chebyshev polynomials was proposed. This method provides a more convenient parameter update formulation that can be used with the the GuAPE method, which is proposed as a way to deal with the control aspect of the remote side along with parameter estimation. The Chebyshev approximation with GuAPE scheme was then evaluated on

a simulated teleoperation system. Since practical applications more clearly show the real performance and limitations of a method, initial results from an experiment using GuAPE are presented and discussed in Section 6.1 below. As parameter updates may cause jumps in the haptic feedback, a smooth transition using a Sigmoid function was used in simulation that increased performance during parameter adaptation.

To address unavoidable shortcomings of teleoperated systems in extended delay times, a semi-autonomous assistive control architecture was proposed. This work was successful in demonstrating the practicality of the proposed semi-autonomous framework through a user study that resulted in reduced task completion times, and accurate user intention recognition. As the method is based on an assumed trajectory from a planner, future work is aimed at optimizing the path planning for both static and moving obstacles. This provides an opportunity for increasing the efficiency and utility of semi-autonomous teleoperation. Moreover, this would provide a platform for extending these capabilities to time delayed teleoperation systems with important applications in remote tasks for telesurgery as well as space and hazardous area operations.

6.1 GuAPE Experiment

The adaptive parameter estimation method described in Section 4.4 above was implement in experiment to examine its use in a practical application. The experimental setup is depicted in Fig. 6.1 and consists of a linear actuator in a vertical rig to guide the actuator for contact with a soft silicone block affixed above. The actuator was powered by a Maxon motor with a 3:1 gear ratio and controlled with a current input scaled from a PWM signal sent by the controller. The lead screw on the actuator had a pitch of 2 mm and position feedback was achieved with a linear encoder with a resolution of .0127 mm mounted on the guide rail. A FUTEK load cell mounted between the rig and the linear actuator measured the force exerted by the actuator. A Tiva TM4C123G board running at 1 kHz was used to communicate between the hardware and a control loop in MATLAB over serial at 500 Hz.

Initial results reveal that one immediate limitation is in the integration of the nonlinear swapping and data accumulation filters. As the tuning gains are increase to provide faster convergence and performance, the limit in communication speed of the loop causes the integration to become unstable. Therefore, only small gains were used that resulted in long convergence times. The GuAPE was derived with an assumed knowledge of the system, in particular the control matrix. Since the parameter update law $\dot{\hat{\theta}} = \Gamma_\theta(-z_2 b\varphi + \mu)$ is scaled by b, any discrepancies in the B matrix used in the nonlinear swapping filter estimate of $\dot{\hat{x}}$ will affect the parameter update, and cause a scaling issue with respect to the parameters. The motor on the actuator used had too much torque for the small penetration application. This resulted in difficulties selecting control parameters c_1 and c_2 to overcome the deadband and provide the desired response; ultimately, the actuator constantly overshot the desired

Figure 6.1: Experimental test stand for proposed adaptive parameter estimation controller.

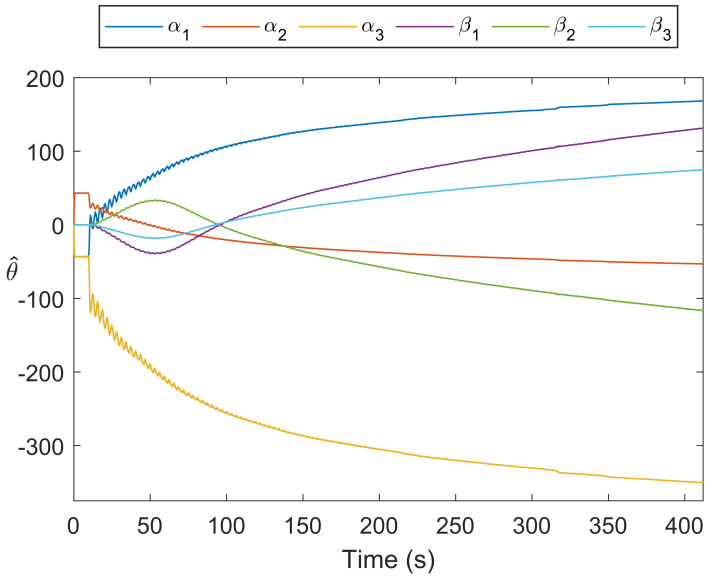

Figure 6.2: Plot of parameter convergence.

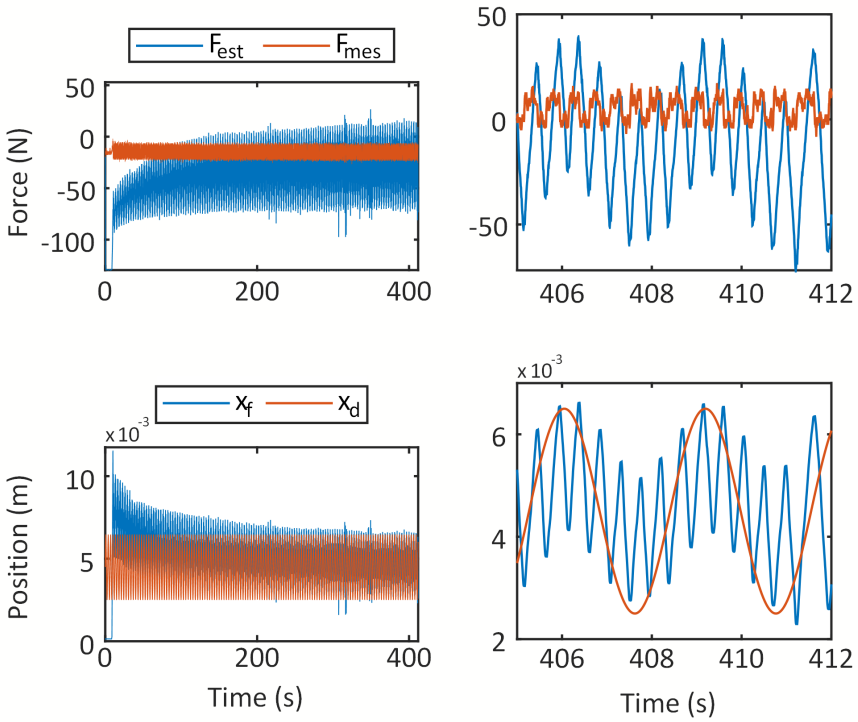

Figure 6.3: Estimated force and position output of the linear actuator compared to the measured force and desired position, with a close up of the last 5 seconds on the right.

trajectory. Because of this, the error system did not achieve asymptotic convergence to zero, but remained bounded as shown in Fig. 6.3. Thus, due to limitations stemming from the hardware, accurate trajectory tracking was not possible and parameter convergence was negatively affected. Although initial result are not ideal from the hardware implementation, the trajectory error does head towards zero and despite taking a long time for parameter convergence, the parameter adaptation follows a path that makes the estimates head toward the measured values with stable behavior as shown in Fig. 6.2. Future work with improvements in the experimental setup, focusing on hardware sizing and using an embedded controller with a more robust integration algorithm, should be pursued to properly evaluate the use of the GuAPE method in real application.

Bibliography

[1] P. F. Hokayem and M. W. Spong, "Bilateral teleoperation: An historical survey," *Automatica*, vol. 42, pp. 2035–2057, 12 2006.

[2] R. Uddin and J. Ryu, "Predictive control approaches for bilateral teleoperation," *Annual Reviews in Control*, vol. 42, pp. 82–99, 2016.

[3] S. Munir and W. Book, "Internet-based teleoperation using wave variables with prediction," *IEEE/ASME Transactions on Mechatronics*, vol. 7, pp. 124–133, 6 2002.

[4] P. Fraisse, B. L. D. Vinci, and A. Einstein, "Teleoperation Over IP Network : Network Delay," pp. 225–235, 2003.

[5] E. Kamrani, "Real-Time Internet-Based Teleoperation," *Intelligent Control and Automation*, vol. 03, no. 04, pp. 356–375, 2012.

[6] W. Kim, B. Hannaford, and A. Fejczy, "Force-reflection and shared compliant control in operating telemanipulators with time delay," *IEEE Transactions on Robotics and Automation*, vol. 8, pp. 176–185, 4 1992.

[7] D. Lawrence, "Stability and transparency in bilateral teleoperation," *IEEE Transactions on Robotics and Automation*, vol. 9, no. 5, pp. 624–637, 1993.

[8] R. Anderson and M. Spong, "Bilateral control of teleoperators with time delay," *IEEE Transactions on Automatic Control*, vol. 34, pp. 494–501, 5 1989.

[9] G. Niemeyer and J.-J. E. Slotine, "Telemanipulation with Time Delays," *The International Journal of Robotics Research*, vol. 23, pp. 873–890, 9 2004.

[10] D. Lee and M. Spong, "Passive Bilateral Teleoperation With Constant Time Delay," *IEEE Transactions on Robotics*, vol. 22, pp. 269–281, 4 2006.

[11] K. Mima, M. Honda, T. Miyoshi, T. Imamura, M. Okabe, F. M. Yazadi, and K. Terashima, "Telemanipulation with a humanoid robot hand/arm between USA and Japan," in *2013 IEEE International Conference on Robotics and Automation*, pp. 3618–3624, IEEE, 5 2013.

[12] C. Smith and P. Jensfelt, "A predictor for operator input for time-delayed teleoperation," *Mechatronics*, vol. 20, pp. 778–786, 10 2010.

[13] U. J. Na, "A new impedance force control of a haptic teleoperation system for improved transparency," *Journal of Mechanical Science and Technology*, vol. 31, pp. 6005–6017, 12 2017.

[14] SMITH and O. J. M., "Closed Control of Loop with Dead Time," *Chemical Engineering Progress*, vol. 53, pp. 217–219, 1957.

[15] A. C. Smith and K. Hashtrudi-Zaad, "Smith Predictor Type Control Architectures for Time Delayed Teleoperation," *The International Journal of Robotics Research*, vol. 25, pp. 797–818, 8 2006.

[16] H. J. Choi and S. Jung, "Neural network-based Smith predictor design for the time-delay in a tele-operated control system," *Artificial Life and Robotics*, vol. 14, pp. 578–583, 12 2009.

[17] K. Hosseini-Suny, H. Momeni, and F. Janabi-Sharifi, "Model Reference Adaptive Control Design for a Teleoperation System with Output Prediction," *Journal of Intelligent & Robotic Systems*, vol. 59, pp. 319–339, 9 2010.

[18] Y. Yang, H. Li, Y. Chen, and J. Yi, "Model Predictive Control for Space Teleoperation Systems Based on a Mixed-H2/H∞ Approach," *Journal of Aerospace Engineering*, vol. 28, p. 04014133, 9 2015.

[19] L. Chan, F. Naghdy, and D. Stirling, "Position and force tracking for non-linear haptic telemanipulator under varying delays with an improved extended active observer," *Robotics and Autonomous Systems*, vol. 75, pp. 145–160, 1 2016.

[20] C. Seo, J.-P. Kim, J. Kim, H.-S. Ahn, and J. Ryu, "Robustly stable bilateral teleoperation under time-varying delays and data losses: an energy-bounding approach," *Journal of Mechanical Science and Technology*, vol. 25, pp. 2089–2100, 8 2011.

[21] R. Uddin, S. Park, and J. Ryu, "A predictive energy-bounding approach for Haptic teleoperation," *Mechatronics*, vol. 35, pp. 148–161, 5 2016.

[22] Y. Yang, C. Hua, and X. Guan, "Finite Time Control Design for Bilateral Teleoperation System With Position Synchronization Error Constrained," *IEEE Transactions on Cybernetics*, vol. 46, pp. 609–619, 3 2016.

[23] J. M. Daly and D. W. L. Wang, "Time-Delayed Output Feedback Bilateral Teleoperation With Force Estimation for n-DOF Nonlinear Manipulators," *IEEE Transactions on Control Systems Technology*, vol. 22, pp. 299–306, 1 2014.

[24] Rui Cortesao, Jaeheung Park, and O. Khatib, "Real-time adaptive control for haptic manipulation with active observers," in *Proceedings 2003 IEEE/RSJ International Conference on Intelligent Robots and Systems (IROS 2003)*, vol. 3, pp. 2938–2943, IEEE, 2003.

[25] J. Song, Y. Ding, Z. Shang, and J. Liang, "Model-mediated teleoperation with improved stability," *International Journal of Advanced Robotic Systems*, vol. 15, p. 172988141876113, 3 2018.

[26] K. H. Hunt and F. R. E. Crossley, "Coefficient of Restitution Interpreted as Damping in Vibroimpact," *Journal of Applied Mechanics*, vol. 42, pp. 440–445, 6 1975.

[27] A. Achhammer, C. Weber, A. Peer, and M. Buss, "Improvement of model-mediated teleoperation using a new hybrid environment estimation technique," in *2010 IEEE International Conference on Robotics and Automation*, pp. 5358–5363, IEEE, 5 2010.

[28] A. Haddadi and K. Hashtrudi-Zaad, "A New Method for Online Parameter Estimation of Hunt-Crossley Environment Dynamic Models," in *2008 IEEE/RSJ International Conference on Intelligent Robots and Systems*, pp. 981–986, IEEE, 9 2008.

[29] A. Haddadi and K. Hashtrudi-Zaad, "Real-Time Identification of Hunt–Crossley Dynamic Models of Contact Environments," *IEEE Transactions on Robotics*, vol. 28, pp. 555–566, 6 2012.

[30] J. Ma, L. Qian, and G. Chen, "Parameter estimation of the Lankarani-Nikravesh contact force model using a new modified linear method," in *2015 IEEE International Conference on Advanced Intelligent Mechatronics (AIM)*, vol. 2015-Augus, pp. 494–499, IEEE, 7 2015.

[31] R. Schindeler and K. Hashtrudi-Zaad, "Online Identification of Environment Hunt–Crossley Models Using Polynomial Linearization," *IEEE Transactions on Robotics*, vol. 34, pp. 447–458, 4 2018.

[32] A. Sie, M. Winek, and T. M. Kowalewski, "Online identification of abdominal tissues in vivo for tissue-aware and injury-avoiding surgical robots," in *2014 IEEE/RSJ International Conference on Intelligent Robots and Systems*, pp. 2036–2042, IEEE, 9 2014.

[33] J. Shin, Y. Zhong, D. Oetomo, and C. Gu, "Random Weighting, Strong Tracking, and Unscented Kalman Filter for Soft Tissue Characterization," *Sensors*, vol. 18, p. 1650, 5 2018.

[34] M. Krstic and P. Kokotovic, "Adaptive nonlinear design with controller-identifier separation and swapping," *IEEE Transactions on Automatic Control*, vol. 40, pp. 426–440, 3 1995.

[35] R. Mishkov and S. Darmonski, "NONLINEAR ADAPTIVE CONTROL AND EXACT PARAMETER ESTIMATION," in *International Conference AUTOMATICS AND INFORMATICS'2013 3-7 October 2013, Sofia, Bulgaria*, no. October, pp. 285–288, 2013.

[36] D. E. Whitney, "Quasi-Static Assembly of Compliantly Supported Rigid Parts," *Journal of Dynamic Systems, Measurement, and Control*, vol. 104, pp. 65–77, 3 1982.

[37] G. A. Pratt, M. M. Williamson, P. Dillworth, J. Pratt, and A. Wright, "Stiffness isn't everything," in *Experimental Robotics IV*, pp. 253–262, London: Springer-Verlag, 1995.

[38] J. Pratt, B. Krupp, and C. Morse, "Series elastic actuators for high fidelity force control," *Industrial Robot: An International Journal*, vol. 29, pp. 234–241, 6 2002.

[39] K. Bodie, C. D. Bellicoso, and M. Hutter, "ANYpulator: Design and control of a safe robotic arm," in *2016 IEEE/RSJ International Conference on Intelligent Robots and Systems (IROS)*, vol. 2016-Novem, pp. 1119–1125, IEEE, 10 2016.

[40] M. Aiple and A. Schiele, "Towards teleoperation with human-like dynamics: Human use of elastic tools," in *2017 IEEE World Haptics Conference (WHC)*, pp. 171–176, IEEE, 6 2017.

[41] C.-H. King, M. D. Killpack, and C. C. Kemp, "Effects of Force Feedback and Arm Compliance on Teleoperation for a Hygiene Task," in *Lecture Notes in Computer Science (including subseries Lecture Notes in Artificial Intelligence and Lecture Notes in Bioinformatics)*, vol. 6191 LNCS, pp. 248–255, 2010.

[42] N. Amirshirzad, A. Kumru, and E. Oztop, "Human Adaptation to Human–Robot Shared Control," *IEEE Transactions on Human-Machine Systems*, vol. PP, pp. 1–11, 2019.

[43] F. Abi-Farraj, C. Pacchierotti, and P. R. Giordano, "User Evaluation of a Haptic-Enabled Shared-Control Approach for Robotic Telemanipulation," in *2018 IEEE/RSJ International Conference on Intelligent Robots and Systems (IROS)*, pp. 1–9, IEEE, 10 2018.

[44] K. Hambuchen, W. Bluethmann, M. Goza, R. Ambrose, K. Wheeler, and K. Rabe, "Towards Supervising Remote Dexterous Robots Across Time Delay," 2006.

[45] K. Landzettel, C. Preusche, A. Albu-Schaffer, D. Reintsema, B. Rebele, and G. Hirzinger, "Robotic On-Orbit Servicing - DLR's Experience and Perspective," in *2006 IEEE/RSJ International Conference on Intelligent Robots and Systems*, pp. 4587–4594, IEEE, 10 2006.

[46] T. Stoyanov, R. Krug, A. Kiselev, D. Sun, and A. Loutfi, "Assisted Telemanipulation: A Stack-Of-Tasks Approach to Remote Manipulator Control," in *2018 IEEE/RSJ International Conference on Intelligent Robots and Systems (IROS)*, pp. 1–9, IEEE, 10 2018.

[47] D.-H. Zhai and Y. Xia, "Adaptive Control of Semi-Autonomous Teleoperation System With Asymmetric Time-Varying Delays and Input Uncertainties," *IEEE Transactions on Cybernetics*, vol. 47, pp. 3621–3633, 11 2017.

[48] X. Wang, C. Yang, H. Ma, and L. Cheng, "Shared control for teleoperation enhanced by autonomous obstacle avoidance of robot manipulator," in *2015 IEEE/RSJ International Conference on Intelligent Robots and Systems (IROS)*, vol. 2015-Decem, pp. 4575–4580, IEEE, 9 2015.

[49] Y.-C. Liu and N. Chopra, "Control of semi-autonomous teleoperation system with time delays," *Automatica*, vol. 49, pp. 1553–1565, 6 2013.

[50] J. Smisek, M. M. van Paassen, and A. Schiele, "Haptic guidance in bilateral teleoperation: Effects of guidance inaccuracy," in *2015 IEEE World Haptics Conference (WHC)*, pp. 500–505, IEEE, 6 2015.

[51] Dong-Gu Kim, Sang-Kyun Kim, Jung-Tae Kim, Chongwon Lee, and Jong-Oh Park, "Active operator guidance using virtual environment in teleoperation," in *Proceedings. 1998 IEEE/RSJ International Conference on Intelligent Robots and Systems. Innovations in Theory, Practice and Applications (Cat. No.98CH36190)*, vol. 2, pp. 1084–1089, IEEE, 1998.

[52] Z. MA and P. Ben-Tzvi, "RML Glove—An Exoskeleton Glove Mechanism With Haptics Feedback," *IEEE/ASME Transactions on Mechatronics*, vol. 20, pp. 641–652, 4 2015.

[53] F. Janabi-Sharifi and I. Hassanzadeh, "Experimental Analysis of Mobile-Robot Teleoperation via Shared Impedance Control," *IEEE Transactions on Systems, Man, and Cybernetics, Part B (Cybernetics)*, vol. 41, pp. 591–606, 4 2011.

[54] N. Diolaiti and C. Melchiorri, "Teleoperation of a mobile robot through haptic feedback," in *IEEE International Workshop HAVE Haptic Virtual Environments and Their*, no. June 2014, pp. 67–72, IEEE, 2002.

[55] P. Aigner and B. McCarragher, "Human integration into robot control utilising potential fields," in *Proceedings of International Conference on Robotics and Automation*, vol. 1, pp. 291–296, IEEE, 1997.

[56] M. Selvaggio, F. Chen, B. Gao, G. Notomista, F. Trapani, and D. Caldwell, "Vision based virtual fixture generation for teleoperated robotic manipulation," in *2016 International Conference on Advanced Robotics and Mechatronics (ICARM)*, pp. 190–195, IEEE, 8 2016.

[57] N. Stefanov, C. Passenberg, A. Peer, and M. Buss, "Design and Evaluation of a Haptic Computer-Assistant for Telemanipulation Tasks," *IEEE Transactions on Human-Machine Systems*, vol. 43, pp. 385–397, 7 2013.

[58] D. Aarno and D. Kragic, "Motion intention recognition in robot assisted applications," *Robotics and Autonomous Systems*, vol. 56, pp. 692–705, 8 2008.

[59] M. J. A. Zeestraten, I. Havoutis, and S. Calinon, "Programming by Demonstration for Shared Control With an Application in Teleoperation," *IEEE Robotics and Automation Letters*, vol. 3, pp. 1848–1855, 7 2018.

[60] H. El-Hussieny, S. F. M. Assal, A. A. Abouelsoud, and S. M. Megahed, "A novel intention prediction strategy for a shared control tele-manipulation system in unknown environments," in *2015 IEEE International Conference on Mechatronics (ICM)*, pp. 204–209, IEEE, 3 2015.

[61] R. J. Chauhan and P. Ben-Tzvi, "Latent Variable Grasp Prediction for Exoskeletal Glove Control," in *Volume 1: Advances in Control Design Methods; Advances in Nonlinear Control; Advances in Robotics; Assistive and Rehabilitation Robotics; Automotive Dynamics and Emerging Powertrain Technologies; Automotive Systems; Bio Engineering Applications; Bio-Mecha*, p. V001T07A002, ASME, 9 2018.

[62] J. Bohren, C. Papazov, D. Burschka, K. Krieger, S. Parusel, S. Haddadin, W. L. Shepherdson, G. D. Hager, and L. L. Whitcomb, "A pilot study in vision-based augmented telemanipulation for remote assembly over high-latency networks," in *2013 IEEE International Conference on Robotics and Automation*, pp. 3631–3638, IEEE, 5 2013.

[63] L. G. Torres, A. Kuntz, H. B. Gilbert, P. J. Swaney, R. J. Hendrick, R. J. Webster, and R. Alterovitz, "A motion planning approach to automatic obstacle avoidance during concentric tube robot teleoperation," in *2015 IEEE International Conference on Robotics and Automation (ICRA)*, vol. 2015-June, pp. 2361–2367, IEEE, 5 2015.

[64] S. Ganjefar, H. Momeni, F. Janabi Sharifi, and M. Hamidi Beheshti, "Behavior of Smith predictor in teleoperation systems with modeling and delay time errors," in *Proceedings of 2003 IEEE Conference on Control Applications, 2003. CCA 2003.*, vol. 2, pp. 1176–1180, IEEE, 2003.

[65] A. Pappalardo, A. Albakri, C. Liu, L. Bascetta, E. De Momi, and P. Poignet, "Hunt–Crossley model based force control for minimally invasive robotic surgery," *Biomedical Signal Processing and Control*, vol. 29, pp. 31–43, 8 2016.

[66] P. Flores and H. M. Lankarani, *Contact Force Models for Multibody Dynamics*, vol. 226 of *Solid Mechanics and Its Applications*. Cham: Springer International Publishing, 2016.

[67] D. A. Jacobs and K. J. Waldron, "Modeling Inelastic Collisions With the Hunt–Crossley Model Using the Energetic Coefficient of Restitution," *Journal of Computational and Nonlinear Dynamics*, vol. 10, p. 021001, 3 2015.

[68] W. Goldsmith, *Impact—The theory and physical behaviour of colliding solids.* London: Edward Arnold Ltd, 1960.

[69] H. Hertz, "Ueber die Beruehrung elastischer Koerper (On Contact Between Elastic Bodies)," *Journal für die reine und angewandte Mathematik*, vol. 171, no. 92, pp. 156–171, 1881.

[70] E. Kreindler and P. Sarachik, "On the concepts of controllability and observability of linear systems," *IEEE Transactions on Automatic Control*, vol. 9, pp. 129–136, 4 1964.

[71] R. Hermann and A. Krener, "Nonlinear controllability and observability," *IEEE Transactions on Automatic Control*, vol. 22, no. 5, pp. 728–740, 1977.

[72] M. Krstic, P. V. Kokotovic, and I. Kanellakopoulos, *Nonlinear and adaptive control design*. John Wiley & Sons, Inc., 1995.

[73] D. Budolak and P. Ben-Tzvi, "Series elastic actuation for improved transparency in time delayed haptic teleoperation," *Mechatronics*, vol. 63, p. 102278, 11 2019.

[74] C. Lee, S. Kwak, J. Kwak, and S. Oh, "Generalization of Series Elastic Actuator Configurations and Dynamic Behavior Comparison," *Actuators*, vol. 6, p. 26, 8 2017.

[75] E. Refour, B. Sebastian, and P. Ben-Tzvi, "Two-Digit Robotic Exoskeleton Glove Mechanism: Design and Integration," *Journal of Mechanisms and Robotics*, vol. 10, p. 025002, 4 2018.

[76] J. Kim and J. Kim, "Viscoelastic Characterization of Mouse Zona Pellucida," *IEEE Transactions on Biomedical Engineering*, vol. 60, pp. 569–575, 2 2013.

[77] M. T. Hagan, H. B. Demuth, M. H. Beale, and O. De Jesús, *Neural Network Design 2nd Edition*. Martin Hagan, 2014, 2 ed., 2014.

[78] D. Budolak, R. Chauhan, and P. Ben-Tzvi, "Semi-Autonomous Teleoperation, Guidance, and Obstacle Avoidance With Path Adherence," in *Volume 5A: 43rd Mechanisms and Robotics Conference*, pp. 1–7, American Society of Mechanical Engineers, 8 2019.

[79] 3D Systems Geomagic Touch Master Haptic Device, "https://www.3dsystems.com/haptics-devices/touch."

[80] KINOVA Robotics MICO 4-DOF Manipulator, "https://www.kinovarobotics.com/en/knowledge-hub/gen2-ultra-lightweight-robot."